UiT
THE ARCTIC
UNIVERSITY
OF NORWAY

Department of Electrical Engineering

Large-scale Wind Power Integration in Northern Norway

Arwinder Singh

Thesis Work for MSc Electrical Engineering, June 2018

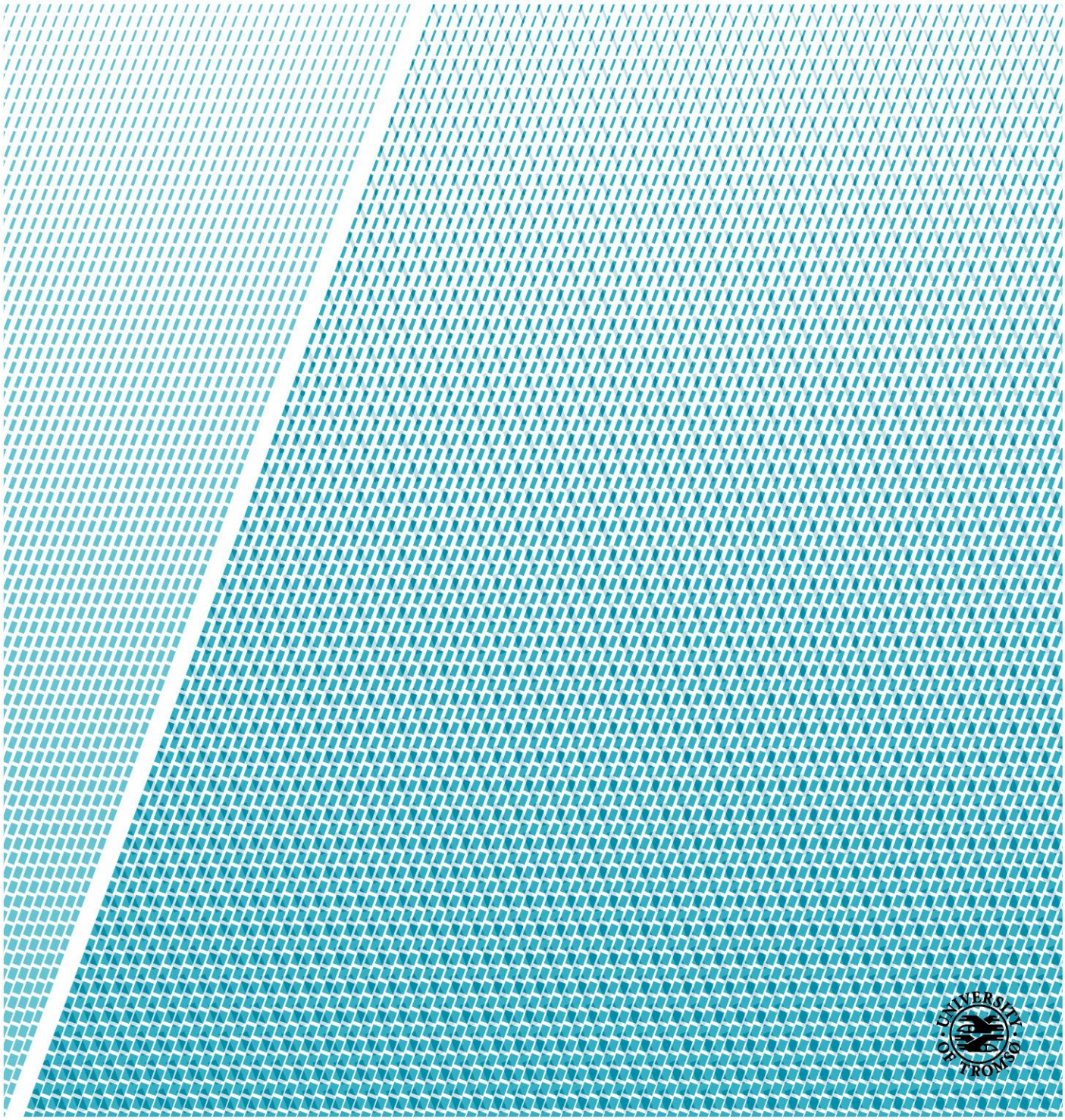

UiT / THE ARCTIC UNIVERSITY OF NORWAY

Title:	*Date:*
Large-scale Wind Power Integration in Northern Norway	June 11, 2018
	Classification:
	Open
Author:	*Pages:*
Arwinder Singh	*67*
	Attachments:
	1

Department:	Institutt for elektroteknologi
Field of Study:	Electrical Engineering
Supervisor:	Terje Gjengedal
Principal:	UiT – The Arctic University of Norway (Campus Narvik)
Principal contact:	Terje Gjengedal
Keywords:	Large-scale Wind Power, Grid Integration, Wind Turbine, Wind Energy Conversion System, Squirrel Cage Induction Generator, Two-level Voltage Source Converter

Acknowledgments

I would like to thank my supervisor, Professor Terje Gjengedal for his help and support throughout this thesis work. Moreover, I would like to take this opportunity to thank all the faculty members of Department of Electrical Engineering for their help and guidance during my master study in Narvik.

I express my gratitude to my family for their affection and support. I dedicate this work to the memory of my mother, Manjit Kaur, who always believed in my ability to be successful in the academic arena. You are gone, but your belief in me has made this journey possible.

Moreover, I am thankful to my friends especially, Bhushan Nikumbh, Aniket Patil, and Brian Dsouza for their constant support and motivational talks.

Arwinder Singh

June 2018

Abstract

Norway has very high flexibility in energy production since hydropower covers about 95% of yearly energy demand. Wind energy is gaining popularity among renewable energy domain. Moreover, Norway has full potential to be leading actor in wind power generation. It is recommended to have a combination of wind power and hydropower, and it applies perfectly here in Norway. In 2012, Norway had a wind energy production of 1.6 GWh. Country approved spending of 20 billion NOK to triple its wind power capacity of around 700 MW to more than 2 GW by 2020 in the following year.

Wind energy production has many benefits over conventional power plants. However, it has few adverse effects on power system's reliability when integrating into the grid, such as transmission congestion, increased balancing requirements for supply and demand and operational efficiency of a power plant using other production technologies. Nevertheless, many projects are running to upgrade transmission lines in Northern Norway and hence increase transmission capacity especially 420 kV Balsfjord - Skillemoen interconnector in western Finnmark. Considerable resource potential is present in this region which requires new grid investments. Several plans for both new consumption and the new generation are also required. Moreover, several interconnectors between neighboring countries are being built to balance the demand and supply curve by constructing a super grid in Europe. The best example to mention here is the upcoming North Sea Link (NSL) between Norway and the UK.

The performance of the wind farm can be significantly enhanced by employing full-capacity converters. The state-of-the-art literature study has been done on Squirrel Cage Induction Generator connected to the grid via two-level voltage source converter. The thesis is further focused on modeling a wind farm as a single machine equivalent to provide 100 MW to the grid by having a best possible way to integrate it into the regional grid of Northern Norway. The primary attention was given to Power converter and Squirrel Cage Induction Generator as they are main electrical components. Mathematical models of induction generator and power converter are studied in depth emphasizes on optimal ways of controlling mechanism.

Analysis of grid connection methods is focused primarily based on Northern Norway grid's voltage rating. However, these schemes can be modified according to the advancement of a transmission system shortly. Steady-state analysis of the system is properly performed. Five case studies are presented which were performed in DIgSILENT © PowerFactory software, and results are examined and discussed. Finally, the discussion and conclusion have been presented.

Abbreviations

WECS	Wind Energy Conversion System
WT	Wind Turbine
WTG	Wind Turbine Generator
HAWT	Horizontal-Axis Wind Turbine
VAWT	Vertical- Axis Wind Turbine
LVRT	Low-Voltage Ride Through
SCIG	Squirrel Cage Induction Generator
2L-VSC	Two-level Voltage Source Converters
VOC	Voltage Oriented Control
VSC	Voltage Source Converters
TSOs	Transmission System Operators
FOC	Field Oriented Control
WES	Wind Energy System

Contents

List of Figures

List of Tables

1 Introduction

1.1 Background and Motivation

There has been a continuous enhancement of power generation from non-conventional to renewable energy sources in recent years. Especially, Wind is one of the most prominent sources of electrical energy. Increasing environmental issues demand the search for more sustainable energy sources. Wind along with solar energy and fuel cells are possible solutions for eco-friendly energy production [1]. Moreover, renewable energy sources are intermittent, except for biomass and geothermal. However, a renewable energy dominated power system can cause concerns related to system stability and reliability. Primarily, the increasing wind power penetration with its uncertain production on all time scales mostly affects the system operation [2].

Norway, once known as Europe's largest oil & gas producer, is making a remarkable transition towards renewable energy. The nation has been the giant producer of renewables for several years, mainly because of numerous hydropower plants across the country. There has been a substantial movement away from the oil & gas sector over last few years. Recently, some of the largest Scandinavian actors, like previous known as Dong Energy (now Ørsted) and Norwegian entity Statoil (now Equinor) have joined this movement. Also, the residents of Scandinavia are highly aware of climate-sensitive issues and always be ready to protect nature.

Norway has become a pivot for green investors from Europe, and several large players are investing in the country's expansion of onshore wind power. In 2012, Norway had a capacity of 700MW, and the goal is to increase it to 2GW by 2020. Fortunately, it seems like the country is well on its way. The owners of Fosen Vind, Norwegian utilities Statkraft and Trønder Energi, and the European consortium Nordic Wind Power DA had been granted concession in 2016. The whole project will consist of 278 turbines in six wind parks. Danish company Vestas will deliver all turbines, and Norwegian subsidiary of Peikko Group will be in charge of the foundation [3].

Norway has a consistent regional and national grid structure. Both local developers and investors are involved in the mix. Moreover, Swedish Eolus Vind and Nordisk Vindkraft (a subsidiary of RES) are in the market. Eolus is developing Øyfjellet in Nordland and Nordisk Vindkraft working on the Buheii project in Vest Agder shire. In addendum, large European developers have realized the potential of

Norway, and firms such as Italian based Falck Renewables and Swiss Scanenergy are developing projects in Northern Norway. Norway is on track and becoming an increasingly sustainable country.

1.2 Wind Farms in Norway

According to [4], Norway is one of biggest hydropower producer in the world. In 2016, 144 TWh energy was produced from hydropower plants [5]. Moreover, Norway is also one of the best-situated European countries for wind power [6]. In 2017, wind contributed 2.85 TWh of energy out of the total installed capacity which stands at 1188 MW spreading over 468 wind turbines. It accounts for 1.9% of the total overall power production, and 0.5% energy production increased concerning 2016 [7].

Table 1-1 Norwegian Measured Wind Power production in 2017* [7]

Wind Power Plant	**Owner**	**Year in Operat-ion**	**No. of Tur-bines**	**Installed capacity (in MW)**	**2017 Produc-tion (in GWh)**
Andøya	Andøya Energi AS	1991	1	0.4	0.5
Fjeldskår	Norsk Miljø Energi AS	1998	5	3.8	4.8
Harøy, Sandøy	Sandøy Energi AS	1999	5	3.8	8.9
Smøla I & II	Smøla Vind AS (Statkraft)	2002	68	150.4	358.5
Havøygavlen	Arctic Wind AS	2002	16	40.5	90.3
Utsira I & II	Solvind Prosjekt AS	2004	2	1.2	3.9
Hitra	Hitra Vind AS (Statkraft)	2004	24	55.2	141.7
Nygårdsfjellet I & II	Nygårdsfjellet Vindpark AS	2005	14	32.2	97.5
Kjøllefjord	Kjøllefjord Vind AS (Statkraft)	2006	17	39.1	107.7
Valsneset	TrønderEnergi Kraft AS	2006	5	11.5	33.7
Bessakerfjellet	TrønderEnergi Kraft AS	2008	25	57.5	164.3
Mehuken II & III	Kvalheim Kraft AS	2010	11	25.3	68.3
Høg-Jæren I & II	Jæren Energi AS	2011	32	73.6	239.0
Åsen II	Solvind Åsen AS	2012	2	1.6	4.2
Fakken	Troms Kraft AS	2012	18	54.0	133.5
Ytre Vikna	Sarepta Energi AS	2012	17	39.1	116.2
Lista	Lista Vindkraftverk AS	2012	31	71.3	238.7
Midtfjellet	Midtfjellet Vindkraft AS	2013	44	110.0	324.8
Raggavidda	Varanger Kraft AS	2014	15	45.0	190.8

Røyrmyra	Røyrmyra Vindpark AS	2015	3	2.4	8.2
Skomakerfjellet	TrønderEnergi Kraft AS	2015	4	13.2	37.9
Other Wind Power	-	-	109	357.1	475.2
Total	**-**	**-**	**468**	**1188**	**2849**

* Wind Power Plants, which were not in normal operation in 2017, are summed up under Other Wind Power Category

1.3 Objectives

The primary objectives of this thesis are:

1. Study the system requirements for Wind Power Plants (Grid Code)
2. Study of Large-scale Wind Power System
3. Study different wind turbine technologies and to choose best possible option
4. Study ways of integrating Wind Power System into the main grid
5. Analyse different problems and constraints which arise due to grid integration of Wind Farm. Therefore, methods will be developed to overcome them.
6. Examine Wind Power Capacity versus Transmission Capacity
7. Modeling the system to achieve Simulation and Results

1.4 Thesis Outline

In chapter 1 of thesis gives background and motivation that has formed the basis for the work. Primary objectives of the thesis have also been presented in this chapter.

Chapter 2 covers the literature study required to make the base of the work.

Chapter 3 includes the modeling of the Induction Generator especially the Squirrel Cage Induction Generator and control scheme of SCIG.

Chapter 4 focuses the control system design of the two-level voltage source converter. It also provides mathematical model used in this study.

Chapter 5 presents the analysis of different case studies performed.

Finally, chapter 6 concludes the thesis by summarizing all accomplished tasks and gives the direction for future work.

2 Literature Study

2.1 Wind Turbines

Wind turbines harvest electricity by using the power of the wind to drive an electrical generator. Wind passes over the blades which generate lift and applies a rotating force. The rotating blades turn a shaft, which goes to a gearbox. The gearbox increases the rotational speed which is appropriate for the generator. Then, the generator uses magnetic fields to convert the rotational energy into electrical energy. The voltage at which power produced by the generator is then stepped up through transformers to the appropriate voltage for the power collection system, typically 66 kV or 132kV in Norway.

2.1.1 Horizontal- and Vertical-Axis Wind Turbines

Wind turbines can be characterized based on the alignment of their spin axis into horizontal-axis wind turbines (HAWT) and vertical-axis wind turbines (VAWT) [8], as shown in Figure 2-1. In horizontal-axis wind turbines, the orientation of the spin axis is parallel to the ground. The tower elevates the nacelle to provide sufficient space for the rotor blade rotation and to reach better wind conditions. The nacelle supports the rotor hub that holds the rotor blades and houses the gearbox, generator, and, in some designs, power converters. The industry standard HAWT uses a three-blade rotor positioned in front of the nacelle, which is known as an upwind formation. However, downwind formations with the blades at the back can also be found in practical applications. Turbines with one, two, or added than three blades can also be seen in wind farms. In vertical-axis wind turbines, the orientation of the spin axis is perpendicular to the ground. The turbine rotor uses curved vertically mounted airfoils. The generator and gearbox are usually placed in the base of the turbine on the ground.

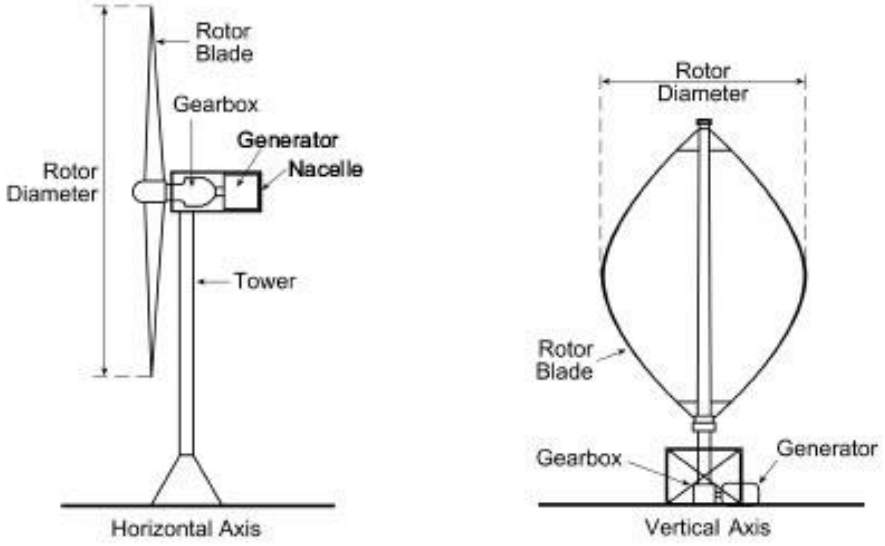

Figure 2-1 Horizontal- and vertical-axis wind turbines [9]

The rotor blades of the Vertical-Axis WT have a variety of designs with different forms and number of blades. The design given in Figure 2-1 is one of the favorite designs. The VAWT needs typically guide wires to keep the rotor shaft in a fixed position and minimize possible mechanical vibrations. A comparison between the horizontal- and vertical-axis turbine technologies are summarized in Table 2-1. The higher wind energy conversion efficiency of Horizontal-Axis WT is due to its blade design and access to stronger wind. However, HAWT needs a stronger tower to support the heavy weight of the nacelle, and its installation cost is higher. On the contrary, the VAWT has the advantage of lower installation costs and easier maintenance due to the ground-level gearbox and generator installation. However, its wind energy conversion efficiency is lower due to the weaker wind on the lower portion of the blades and limited aerodynamic performance of the blades. Also, the rotor shaft is long, making it prone to mechanical vibrations. These disadvantages hinder the practical application of vertical-axis turbines for large-scale wind energy conversion. Horizontal-axis turbines dominate today's wind market, especially in large commercial wind farms.

Table 2-1 Comparison between horizontal- and vertical-axis wind turbines [9]

HAWT	
Advantages	Disadvantages
• Higher wind energy conversion efficiency • Access to stronger wind due to a high tower • Power regulation by stall and pitch angle control at high wind speeds	• Higher installation cost, stronger tower to support the heavy weight of the nacelle • Longer cable from the top of the tower to the ground • Orientation required (yaw control)
VAWT	
Advantages	Disadvantages
• Lower installation cost and easier maintenance due to the ground-level gearbox and generator • Operation independent of wind direction • Suitable for rooftops (stronger wind without the need of tower)	• Lower wind energy conversion efficiency • Higher torque fluctuations and prone to mechanical vibrations • Limited options for power regulation at high wind speeds

2.1.2 Fixed- and Variable-Speed Turbines

Wind turbines can also be categorized into fixed-speed and variable-speed turbines. Fixed-speed wind turbines rotate nearly at a constant speed, which is determined mainly by the grid frequency, the gear ratio and the number of poles of the generator. The maximum conversion efficiency can be attained only at given wind speed. However, system efficiency degrades at other wind speeds [10]. To protect from probable harm of high wind gusts, aerodynamic control of the blades is used. Power system experiences disturbance due to highly fluctuating nature of output power of the fixed-speed turbine to the grid. This type of turbine also entails a robust mechanical design to absorb high mechanical stresses [11].

On the other hand, variable-speed wind turbines can achieve maximum energy conversion efficiency over a wide range of wind speeds. The turbine can continuously regulate its rotating speed concerning the wind speed. In doing so, the tip speed ratio (λ_T) can be kept at an optimum value to achieve the maximum power conversion efficiency at different wind speeds [8].

To make the turbine's speed adjustable, the wind turbine generator is usually connected to the utility grid through a power converter system [10]. The generator is mechanically coupled to the rotor (blades) of the wind turbine, and the converter system enables the speed controller of the generator. As shown in Table 2-2, the main advantages of the variable-speed turbine include increased wind energy output, improved power quality, and reduced mechanical stress [11]. The main disadvantages are the high manufacturing price and power losses due to the usage of power converters. However, the additional cost and power losses are compensated for by the higher energy production. Furthermore, the smoother operation provided by the controlled generator reduces mechanical stress on the turbine, the drive train and the supporting structure. This has enabled manufacturers to develop giant wind turbines that are more profitable. Due to the above reasons, variable-speed turbines lead the current market.

Table 2-2 Advantages and drawbacks of fixed- and variable-speed wind turbines [9]

Fixed speed	
Advantages	Disadvantages
• Simple, robust, reliable • Low cost and maintenance efficiency	• Relatively low energy-conversion • High mechanical stress • High power fluctuations to the grid
Variable speed	

Advantages	Disadvantages
• The high efficiency of energy conversion • Enhanced power quality • Reduced mechanical stress	• Added expense and losses due to the usage of converters • The more complex control system

2.2 Wind Turbine Generators

Generators are used to perform the conversion of rotational mechanical energy to electrical energy. There are different types of the generator which have been used in wind energy systems over the years, e.g., squirrel cage induction generator (SCIG), doubly fed induction generator (DFIG), and synchronous generator (SG) (wound rotor and permanent magnet). These have power ratings from a few kilowatts to several megawatts [12].

The popularity of induction generator has increased tremendously in the application within renewable energy sources. Induction generator advantages include ruggedness, brushless (in squirrel cage construction), the absence of separate DC source for excitation, easy maintenance, self-protection against severe overloads and short circuits, and so forth. These advantages make them preferable over another generator in some applications. Induction generator does not need frequency control equipment and has low initial investment and maintenance cost [13]. A significant drawback of induction generator is its poor performance regarding voltage regulation as it requires a magnetizing current from the source of excitation. However, this drawback can be eliminated by using full-capacity power converters. The combination of squirrel cage induction generator (SCIG) wind energy conversion system (WECS) and full-capacity power converters is dominating the market in contemporary times.

The DFIG plays a significant role in wind energy industry. The stator terminals of the generator are connected directly to the grid, while the rotor is interfaced with the grid through a reduced capacity power converter system. DFIG is adequate for most wind speed conditions because it operates typically about 30% above and below synchronous speed [9]. It also permits generator-side active power control and grid-side reactive power control.

The synchronous generator is very well-matched for direct-drive wind turbines [9]. Permanent magnet generators are preferred in recent trends as they are having higher efficiency and power density as compared to wound rotor generators.

2.3 Wind Energy Conversion System (WECS) Arrangements

Power converter and the generator are two principal electrical components in a WECS. Different designs and groupings of these two components make possible a wide variety of WECS arrangements [10], which can be classified into three groups:

1. Fixed-speed WECS without power converter interface
2. WECS using reduced-capacity converters
3. Full-capacity converter operated WECS

2.3.1 Fixed-Speed WECS without Power Converter Interface

A typical configuration of WECS without a power converter interface is shown in Figure 2-2, in which the generator is coupled to the grid through a transformer. A squirrel cage induction generator (SCIG) is hugely used in this type of WECS, and its rotating speed is determined by the grid frequency and the number of poles of the stator winding. For a four-pole megawatt generator connected to a grid of 50 Hz, the generator operates at speed slightly higher than 1500 rpm. The generator speed varies within 1% of its rated speed at different wind speeds. The generator's range of speed is so small that this system is often known as a fixed-speed WECS [9].

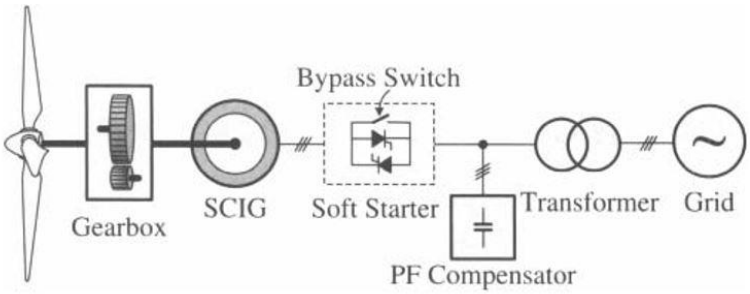

Figure 2-2 WECS without power converter interface [9]

A gearbox is usually required to match the speed change between the turbine and generator such that the generator can produce rated power at the rated wind speed. This configuration needs a soft starter to limit high inrush currents during system start-up, but a switch bypasses the soft starter after the system is started. During normal operation, the system does not want any power converter. A three-phase capacitor bank is usually required to compensate for the reactive power drawn by the induction generator.

This wind energy system features simplicity, low manufacturing/maintenance costs, and reliable operation.

The main drawbacks include:

1. the system transfers the rated power to the grid only at given wind speed, leading to low energy conversion efficiency at other wind speeds
2. the power transferred to the grid fluctuates with the wind speed, causing disturbances to the grid

Despite its disadvantages, this wind energy system is still widely accepted in the industry with a power rating of up to a couple of megawatts.

2.3.2 Variable-Speed Systems with Reduced-Capacity Converters

The variable-speed operation has many advantages over fixed-speed wind systems. It raises the energy conversion efficiency and reduces mechanical stress caused by wind gusts. The latter has a positive impact on the design of the structure and mechanical parts of the turbine and enables the construction of giant wind turbines. It also reduces the wear and tears on the gearbox and bearings, increasing the life cycle and reducing the maintenance requirements. The main disadvantage of variable-speed WECS is the need for a power converter interface to control the generator speed, which increases cost and complexity to the system. However, the power converter decouples the generator from the grid, which enables the control of the grid-side active and reactive power [10]. Variable-speed WECS can be further separated into two types based on the power rating of the converter concerning the total power of the system: reduced-capacity power converter and a full-capacity power converter. The variable-speed WECS with reduced-capacity converters are only possible with wound-rotor induction generators (WRIG) because the variable-speed operation can be attained by controlling the rotor currents without the necessity of processing the full power of the system. Two designs are there for the WRIG configurations**:** (1) with Converter-controlled variable resistance and (2) with Four-quadrant power converter system.

WRIG with Variable Rotor Resistance

Figure 2-3 shows a typical block diagram of the WRIG wind energy system with variable resistance in the rotor circuit. The variation in the rotor resistance affects the torque/speed characteristic of the generator, enabling variable-speed operation of the turbine. The rotor resistance usually is made adaptable by a power converter. The speed adjustment range is typically restricted to about 10% above the synchronous speed of the generator [14]. With the variable-speed operation, the system can capture more power from the wind but also has energy losses in the rotor resistance. This configuration also requires a soft starter and reactive power compensation. The WRIG with variable rotor resistance has been in the market since the mid-1990s with a power rating up to megawatts.

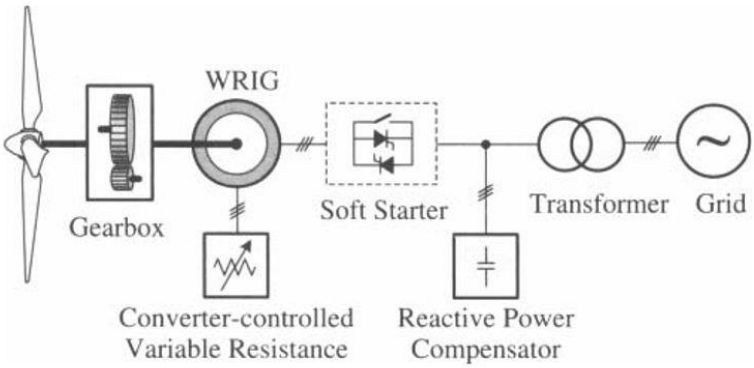

Figure 2-3 Variable-speed configuration with variable rotor resistance [9]

Doubly-Fed Induction Generator with Rotor Converter

A typical block diagram of the doubly-fed induction generator (DFIG) wind energy system is shown in Figure 2-4. The configuration of this system is the identical to WRIG system except (1) the adjustable resistance in the rotor circuit is changed by a grid-connected power converter system, and (2) there is no requirement for the soft starter or reactive power compensation. The power factor of the system can be adjusted by the power converters. The converters must only process the slip power in the rotor circuits, which is around 30% of the rated power of the generator. It lowers the cost of the converter as compared to the WES using full-capacity converters [10].

The use of the converters also allows bi-directional power flow in the rotor circuit and raises the speed range of the generator. This system features enhanced overall power conversion efficiency, extended generator speed range (±30%), and improved dynamic performance in contrast to the fixed-speed WECS and the variable resistance configuration. These attributes have made the DFIG wind energy system broadly accepted in today's market [9].

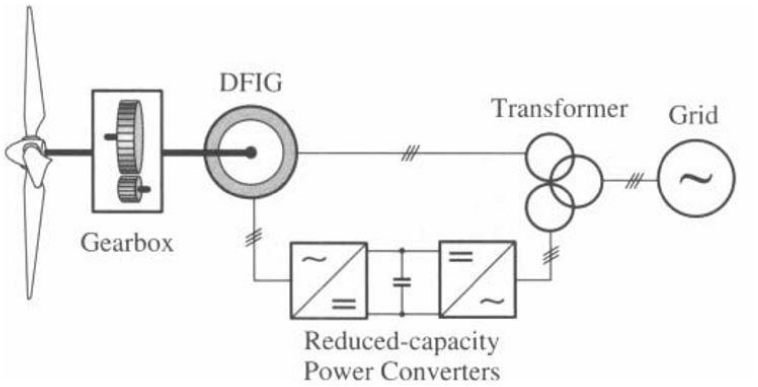

Figure 2-4 Variable-speed configuration with reduced-capacity converters [9]

2.3.3 Variable-Speed Systems with Full-Capacity Power Converters

By using full-capacity power converter, the performance of the WES can be significantly improved. Figure 2-5 shows such a system in which the generator is connected to the grid via a full-capacity converter system [10]. Squirrel cage induction generators, permanent magnet synchronous generators (PMSG), and wound rotor synchronous generators have all found applications in this kind of configuration with a power rating up to several megawatts. The power rating of the converter is usually equal to the generator. The generator is entirely decoupled from the grid by using a power converter. Moreover, it can operate in full speed range. The power converter also enables the system to produce reactive power and smooth the grid connection. The main disadvantage is a more complex system with increased costs.

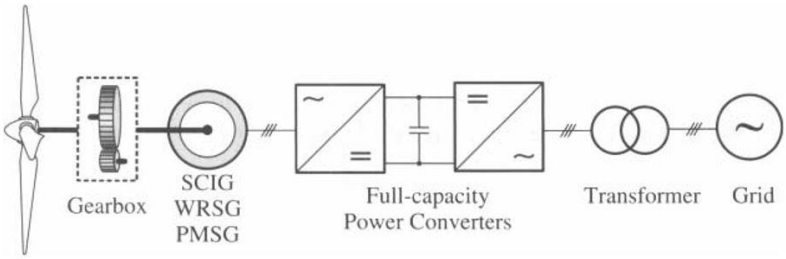

Figure 2-5 Variable-speed configuration with full-capacity converters [9]

It is noted that the WES can operate without the need for a gearbox if a low-speed synchronous generator with many poles is used. The removal of the gearbox improves the efficiency of the system and reduces initial costs and maintenance. Nevertheless, a low-speed generator has a considerably larger diameter to house the large number of poles on the perimeter, which may cause an increase in generator size and installation costs. Some of the most common converter topologies used for this type of WECS include two-level voltage source converter (2L-VSC) in a back-to-back configuration, diode-bridge rectifier plus DC-DC boost stage and 2L-VSC, and three-level neutral point clamped converter (3L-NPC) in a back-to-back configuration.

2.4 Grid Integration of Wind Energy Systems

In Norway, wind farms typically connect to the 66 or 132 kV level transmission lines, usually with a rather low short-circuit power [6]. However, some issues need to consider before the development of large wind power plants in such grids. These include the applied connection to the network, integration with the network system, system stability, sub-synchronous oscillations within the power plant, required installations and extensions of the grid. Turbines usually do not take part in voltage and frequency control for small-scale wind farms. In case of disturbance, the wind turbines are generally disconnected and later reconnected when the regulated operation has resumed.

However, the wind turbines begin to influence the overall power system behavior when the amount of wind power is increasing. Thus, making the power system tough to operate by only controlling other large-scale power plants. It is evident that the level of wind power connects into the system depends severely on the type of system, i.e., short-circuit levels, fast active/reactive power control capabilities, concentrated or distributed generation, grid congestions. Hence, much consideration must be given to detailed system design while developing large-scale wind farms [15].

Progressively, grid operators and regulators specify functional requirements wind farms must meet. Several countries have specified such requirements, including dynamic responses, fault ride-through capability and active and reactive control responses. Specific requirements may be difficult or expensive to meet [6], [16].

The large-scale integration can occur in two primary conditions:

- Large wind farms connected to the transmission system
- Many small wind farms connected to the distribution systems in one area of the power system

In either condition, the assessment of power quality and system stability become more complex; they demand special investigations of voltage and frequency variations depending on the system size. In the small-scale integration, the frequency is assumed to be constant. With high wind power capacity installations, sizeable active power variations can interact with the frequency controllers in the conventional power stations and may result in frequency variations. Also, considerable reactive power demanded by the wind farms can reduce the reactive power supply. Hence, voltage stability limits can be reduced and must be analyzed.

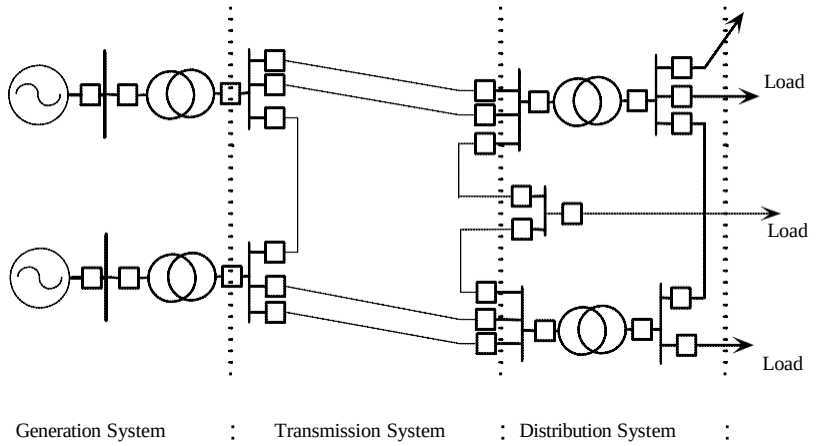

Figure 2-6 Basic Power System Structure [1]

Figure 2-6 presents a simple single line of a fundamental power system structure, where it is possible to distinguish the main system components. The generation system is mostly composed of synchronous

machines that are usually large. The transmission system contains transmission lines that extend for vast distances and connect different generation and distribution units. The transmission lines require attention while controlling the voltage at the terminals due to reactive power flow (in AC type lines). Distribution systems deliver power to the loads at a lower voltage level. The distribution lines need attention while controlling voltage at the loads. The power system must supply a reliable and quality electrical power to the loads. The power system must have enough reserves that can deliver the power when it is required to achieve reliability. Further, active controllers compensate the voltage and frequency variations keeping the power quality within limits.

2.5 Grid connection requirements for wind turbines

In many countries, grid codes have been developed and enforced for many years. They ensure uniform standards for power systems and provide an outline for producers to develop their equipment [9]. In addition to this, they provide a framework for manufacturers to develop their equipment. Grid codes are usually based on the experience attained through the operation of power systems and may differ from one utility to another. In Norway, Nordic Grid code must be followed, and it was updated in 2007 last time. Differences in various grid codes also stem from regional and geographic circumstances. However, the crucial elements in the different grid codes remain similar across the globe since their goal is to ensure the safety, reliability, and economical operation of the power system.

The grid codes in many countries have been updated to address issues related to renewable energy power generation due to the rapid development of the renewable energies and their integration into the grid [17]. According to the updated grid codes, wind farms tend to be considered as power generation plants, which should perform similarly as conventional power-generation plants do.

Fault ride-through requirements, active/reactive power control, frequency/voltage regulation, power quality, and system protection are classified as primary elements in the grid codes. However, fault ride-through requirement and reactive power control are most important to consider.

2.5.1 Fault Ride-Through Requirements

Grid disturbances such as severe voltage dip caused by short-circuiting faults. These can lead to power-generating units disconnected from the grid, which may cause instability in the grid. The grid code requires power-generating units to remain connected and continuously operated even if the voltage dips reaches very low values to avoid instability [18]. A voltage-time diagram usually defines the depth and duration of the voltage dips. Figure 2-7 shows an example of low-voltage ride-through (LVRT) requirements during grid faults, where U_n is the nominal voltage of the grid [19]. Above the limit line, a power-generating system must remain connected during the fault even when the grid voltage falls to zero with duration of less than 150 ms. When the voltage dips are in the area below the limit line, then

only the system can be disconnected from the grid. According to grid codes, the system needs to supply a certain amount of reactive power to support the grid voltage during the fault [20]. Grid codes share a common background and purpose, although Transmission System Operators (TSOs), which is Statnett in Norway, in different countries specify the different limits and ranges for LVRT requirements. Wind Turbines equipped with full-capacity converters fulfill these requirements.

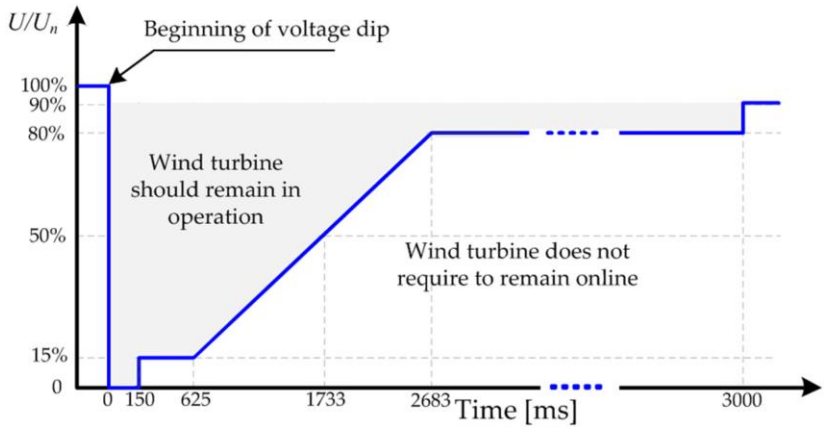

Figure 2-7 Example of grid requirements for low-voltage ride-through [21]

2.5.2 Reactive Power Control

Like the conventional power plants, wind turbines or wind farms are required to provide reactive power to the grid. Figure 2-8 illustrates an example of the range of the reactive power versus the active power for a power-generating unit [17]. A large megawatt wind turbine should be able to produce a maximum reactive power of ±0.33 pu when it deliveries the rated active power (1 pu) to the grid to support voltage of the grid. This relationship corresponds to a 0.95 lagging and leading power factor, respectively.

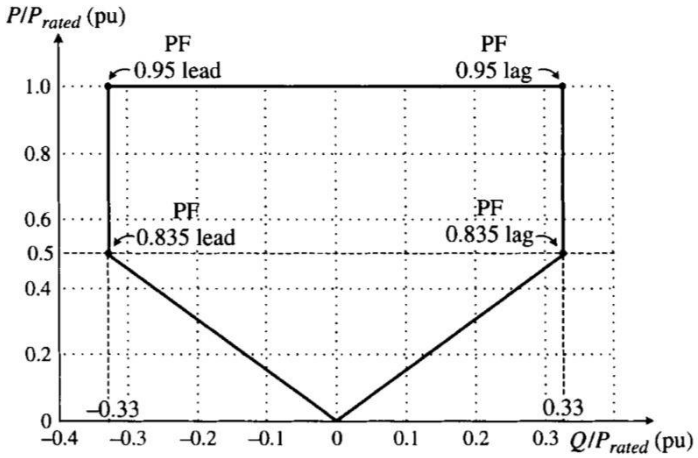

Figure 2-8 Example of reactive power requirements during normal system operation [17]

Similarly, an active power generation of 0.5 pu and capability of providing up to ±0.33 pu reactive power corresponds to a 0.835 lagging and leading power factor, respectively. A properly designed variable-speed WECS can fulfill this requirement. The illustrated scenario may be varied in different grid codes across the globe.

2.6 Wind Power Capacity versus Transmission Capacity

One of the most critical issues for constructing of wind farms in Northern Norway is the transmission capacity of the grid in this area. Like many other countries, wind farms are concentrated in less populated areas, where the existing transmission grids are very weak. Additional transmission capacity is needed to integrate new power generation units. Moreover, wind power has some unique features that must be considered when assessing transmission capacity.

First, wind power production must be evaluated considering its low utilization time (2000–3000 hours per year), the special smoothing effect and the fact that the power output is a function of the ambient conditions [11]. Also, wind power can be treated as any conventional generation when evaluating the thermal limits. Wind speed measurements from wind farms can even be used for the online estimation of the current-carrying capacity of short transmission lines.

The induction generators that are used in wind power applications consume reactive power. If there is no reactive power compensation, this results in a lagging power factor at the wind farm connection point. If voltage stability considerations define the limit, this may decrease the maximum power transfer from the wind farm to the network. Reactive power compensation of wind turbines is generally provided by shunt capacitor banks, SVC or AC/DC/AC converters. Reactive power compensation provided by shunt capacitor banks depends on the voltage at the connection point and therefore may not be sufficient for lower voltage. However, if continuous reactive power compensation is used through AC/DC/AC converters, for example, wind power does not affect the maximum power transfer if voltage stability considerations define the limit. In addition to this, if at the wind farm connection point a leading power factor is provided, the maximum power transfer over the considered line could be increased, especially if it is acceptable to have a higher voltage at the wind farm connection point.

During and after faults in the system, the behavior of wind turbines is different from that of conventional power plants. Conventional power plants mainly use synchronous generators that can continue to operate during severe voltage transients produced by transmission system faults. Variable-speed wind turbines are disconnected from the grid during a fault to protect the converter. If a significant amount of wind generation is tripped because of a fault, the adverse effects of that fault could be magnified [22]. This may affect the transmission capacity in areas with significant amounts of wind power, as a sequence of contingencies would be considered in the security assessment instead of only one contingency. During a fault, fixed-speed wind turbines may draw large amounts of reactive power from the system. Thus, the system may recover much more slowly from the fault.

There are several reasons why the integration of large-scale wind power may have an impact on the methods that are used for determining the available transmission capacity:

- The power output of wind farms depends on wind speed. Therefore TSOs should include wind forecasts in the base case for determining the day-ahead transmission capacity and use wind speed statistics in the base case that is used for determining the Net Transfer Capacity (NTC) twice a year. There may be higher uncertainties associated with prediction errors regarding the generation distribution, and this may result in an increased transmission reliability margin, which in other word corresponds to a decrease in transmission capacity.
- Compared with conventional generation, for wind farms, less sophisticated models of generator characteristics are used. This could make simulation results less reliable (i.e., some TSOs may choose to increase transmission reliability margins to account for that).

Apart from the impact that wind power has on the methods for determining transmission capacity, its integration also requires greater investment regarding some of the measures for achieving an increased transmission capacity. It may be significantly more expensive to provide sophisticated protection schemes for wind farms that are distributed over a specific area than for conventional generation of similar capacity [22]. Wind farms are built in remote areas where the grid reinforcements are more urgent and more expensive. However, conventional generation is usually situated close to industrial loads.

3 Induction Generator Modeling

3.1 Aerodynamic Model

The following well-known equation gives the relation between wind speed and mechanical power extracted from the wind [23]:

$$P_M = \frac{1}{2}\rho A C_p(\lambda_T, \theta) v_w^3 \tag{3.1}$$

where P_M is the power extracted from the wind, ρ is the air density, A is the area covered by the wind turbine rotor, v_w is the wind speed and C_p is the power coefficient, which is a function of the tip speed ratio λ_T and the pitch angle θ. The ratio of the tip speed of the blades to the wind speed at hub height, upstream of the rotor is called the tip speed ratio.

$$\lambda_T = \frac{\omega_M r_T}{v_w} \tag{3.2}$$

Where r_T is the radius of the turbine rotor, and ω_M is the rotating speed of the blade.
A general approximation of the power coefficient is used:

$$C_p = C_1\left(\frac{C_2}{\lambda_i} - C_3\theta - C_4\right)e^{\frac{-C_5}{\lambda_i}} + C_6\lambda \tag{3.3}$$

Where

$$\frac{1}{\lambda_i} = \frac{1}{\lambda + 0.08\theta} - \frac{0.035}{\theta^3 + 1} \tag{3.4}$$

and C_1- C_6 are constants [11].

Since we assume that the wind speed does not change, and that wind turbines produce near their rated power, then the reference speed for the wind turbine is always set to its nominal value.
Equations (3.2) and (3.3) are used to calculate the impact of the pitch angle θ on the power coefficient. The resulting value can be inserted into Equation (3.1) to calculate the mechanical power extracted from the wind.

3.2 Reference Frame Transformation

The reference frame theory is used to make the analysis of electric machines simpler and also to ease the simulation and digital implementation of control schemes in WECS. Some reference frames have been proposed over the years, of which the three-phase stationary frame (also known as abc frame), the two-phase stationary frame (αβ frame), and the synchronous frame (dq rotating frame) are most

commonly used [24]. The transformation of variables between these reference frames is presented below.

3.2.1 abc/dq Reference Frame Transformation

Consider generic three-phase electrical variables, $x_a, x_b,$ and x_c, which can characterize either voltage, current, or flux linkage. The three-phase variables can be represented by a space vector $\vec{x}$ in a three-phase (abc) stationary reference frame (coordinate system). The relationship between the space vector and its three-phase variables is illustrated in Figure 3-1, where the space vector $\vec{x}$ rotates at an arbitrary speed ω with respect to the abc stationary frame. Its phase values, $x_a, x_b,$ and x_c, can be obtained by projecting $\vec{x}$ to the corresponding a-, b-, and c- axes that are 2π/3 apart in space. Since the abc axes are stationary in space, each of the three-phase variables varies one cycle over time when $\vec{x}$ rotates one revolution in space.

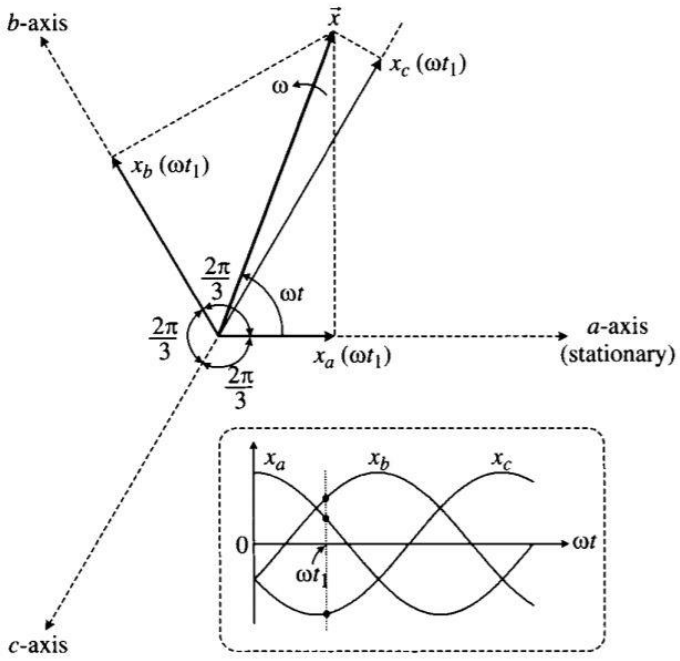

Figure 3-1 Space vector and its three-phase variables [9]

If the length (magnitude) and the rotating speed of space vector $\vec{x}$ are constant, the waveforms of $x_a, x_b,$ and x_c are sinusoidal with a phase displacement of 2π/3 between any two waveforms, as shown in Figure 3-2. The space vector diagram and its corresponding waveforms indicate that at the instant of ωt_1 , x_b is greater than $x_a,$ and x_c is negative.

The three-phase variables in the abc stationary frame can be transformed into two-phase variables in a reference frame defined by the d (direct) and q (quadrature) axes that are perpendicular to each other as

shown in Figure 3-2. The dq-axis frame has an arbitrary position with respect to the abc -axis stationary frame given by the angle θ between the a-axis and d-axis. The dq -axis frame rotates in space at an arbitrary speed ω, which relates to 0 by $\omega = d\theta/dt$.

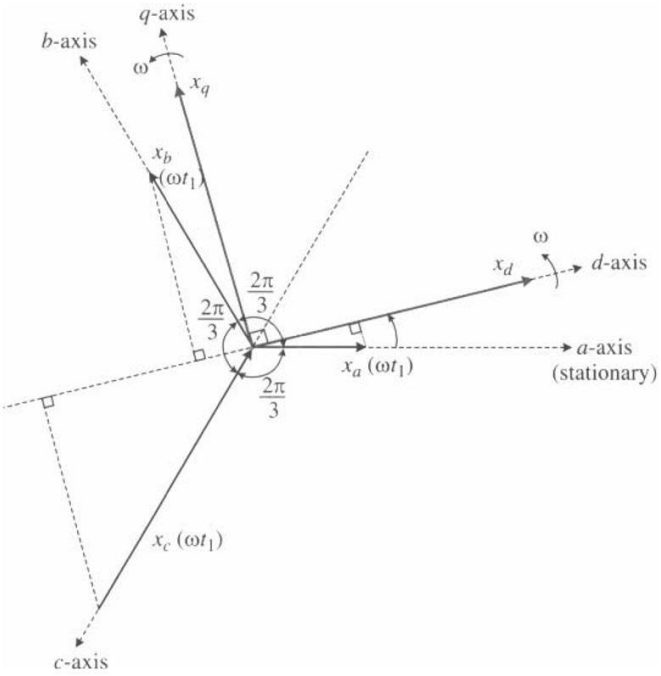

Figure 3-2 Transformation of variables in 3-phase stationary frame to 2-phase arbitrary frame [9]

To transform variables in the abc stationary frame to the dq rotating frame, simple trigonometric functions can be derived from the orthogonal projection of the $x_a, x_b,$ and x_c variables to the dq-axis as shown in Figure 3-2, where only the projections to the d-axis are illustrated.

The sum of all projections on the d-axis corresponds to the transformed x_d, given by $x_d = x_a \cos\theta + x_b \cos(2\pi/3 - \theta) + x_c \cos(4\pi/3 - \theta)$, which can be rewritten as $x_d = x_a \cos\theta + x_b \cos(\theta - 2\pi/3) + x_c \cos(\theta - 4\pi/3)$. Similarly, the transformation of the abc variables into the q-axis can be performed. The transformation of the abc variables to the dq frames, referred to as abc/dq transformation, can be expressed in a matrix form:

$$\begin{bmatrix} x_d \\ x_q \end{bmatrix} = \begin{bmatrix} \cos\theta & \cos(\theta - 2\pi/3) & \cos(\theta - 4\pi/3) \\ -\sin\theta & -\sin(\theta - 2\pi/3) & -\sin(\theta - 4\pi/3) \end{bmatrix} \cdot \begin{bmatrix} x_a \\ x_b \\ x_c \end{bmatrix} \qquad (3.5)$$

It is noted that in the above abc/dq transformation:

- A coefficient of 2/3 is added arbitrarily to the equation. The magnitude of the two-phase voltages is equal to that of the three-phase voltages after the transformation, and this is main benefit of using 2/3.
- The two-phase dq variables after the transformation comprise all the information of the three-phase abc variables. The system must be three-phase balanced in this case. Only two are independent out of the three variables in a three-phase balanced system. Given two independent variables, the third one can be calculated by

$$x_a + x_b + x_c = 0 \tag{3.6}$$

The equations for an inverse transformation can be found by matrix operations, through which the dq variables in the revolving frame can be altered back to the abc variables in the stationary frame. The transformation is known as dq/abc transformation and can be performed by

$$\begin{bmatrix} x_a \\ x_b \\ x_c \end{bmatrix} = \begin{bmatrix} \cos\theta & -\sin\theta \\ \cos(\theta - 2\pi/3) & -\sin(\theta - 2\pi/3) \\ \cos(\theta - 4\pi/3) & -\sin(\theta - 4\pi/3) \end{bmatrix} . \begin{bmatrix} x_d \\ x_q \end{bmatrix} \tag{3.7}$$

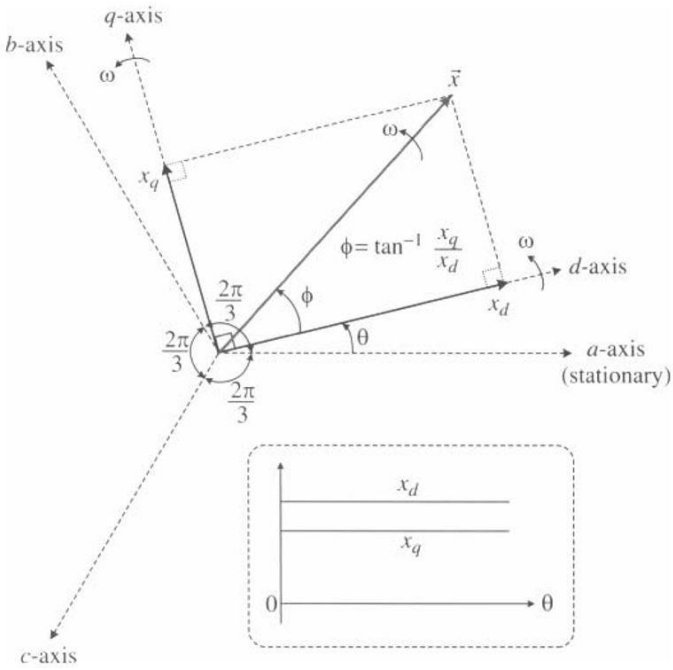

Figure 3-3 Decomposition of space vector into dq rotating reference frame [9]

Figure 3-3 illustrates the decomposition of the space vector $\vec{x}$ into the dq rotating reference frame. Assuming that $\vec{x}$ revolves at the same speed as that of the dq frame, the vector angle ϕ between $\vec{x}$ and the d-axis is constant. The resultant dq-axis components, x_d and x_q, are DC variables. This is one of

the benefits of the abc/dq transformation, whereby three-phase AC variables can be effectively represented by two-phase DC variables.

The synchronous reference frame is commonly used for the control of WES. In this case, the rotating speed of the arbitrary reference frame ω is set to the synchronous speed ω_s of induction or synchronous generator, given by

$$\omega_s = 2\pi f_s \tag{3.8}$$

where f_s is the stator frequency in Hertz. The angle θ can be found from

$$\theta(t) = \int_0^t \omega_s(t) + \theta_0 \tag{3.9}$$

where θ_0 is the initial angular position.

3.2.2 abc/αβ Reference Frame Transformation

The transformation of three-phase variables in the stationary reference frame into the two-phase variables in the stationary frame is generally referred to as abc/αβ transformation. Since the αβ reference frame does not rotate in space, the transformation can be obtained by setting θ in Equation (3.5) to zero, from which

$$\begin{bmatrix} x_\alpha \\ x_\beta \end{bmatrix} = \frac{2}{3}\begin{bmatrix} 1 & -1/2 & -1/2 \\ 0 & \sqrt{3}/2 & -\sqrt{3}/2 \end{bmatrix} . \begin{bmatrix} x_a \\ x_b \\ x_c \end{bmatrix} \tag{3.10}$$

It is alluring to note that in a three-phase balanced system, where $x_a + x_b + x_c = 0$, the relationship between x_a in the αβ reference frame and x_a in the abc frame is given by

$$x_\alpha = \frac{2}{3}\left(x_a - \frac{1}{2}x_b - \frac{1}{2}x_c\right) = x_a \tag{3.11}$$

Similarly, the two-phase to three-phase transformation in the stationary reference frame, known as αβ/abc transformation, can be performed by

$$\begin{bmatrix} x_a \\ x_b \\ x_c \end{bmatrix} = \begin{bmatrix} 1 & 0 \\ -1/2 & \sqrt{3}/2 \\ -1/2 & -\sqrt{3}/2 \end{bmatrix} . \begin{bmatrix} x_\alpha \\ x_\beta \end{bmatrix} \tag{3.12}$$

3.3 Squirrel Cage Induction Generator

The induction machine is the most extensively used electrical machine and has been most commonly used to convert electric power into work. Induction machines have traditionally been used in constant speed applications, but these machines are now also being used in variable speed applications because they are robust and comparatively inexpensive.

It consists of a cylindrical stator with three-phase windings distributed symmetrically around its periphery, and a rotor which is free to rotate inside the stator and is separated from the stator by an air gap. The rotor of the SCIG is composed of the laminated core and rotor bars. The rotor bars are embedded in slots inside the rotor laminations. Also, they are shorted on both ends by end rings. A rotating magnetic field is produced in the air gap when the stator winding is connected to a three-phase supply. The rotating field induces a three-phase voltage in the rotor bars. Since the rotor bars are shorted, the induced rotor voltage produces a rotor current, which interacts with the rotating field to produce the electromagnetic torque.

Figure 3-4a shows the construction of a squirrel-cage induction generator. The stator is made of thin silicon steel laminations. The laminations are insulated to minimize iron losses caused by induced eddy currents. The laminations are flat rings with openings disposed along the inner perimeter of the ring. When the laminations are stacked together with the openings aligned, a canal is formed, in which a three-phase copper winding is placed [9].

A simplified diagram of the induction generator is shown in Figure 3-4b, where the multiple coils in the stator and multiple bars in the rotor are grouped and represented by a single coil for each phase.

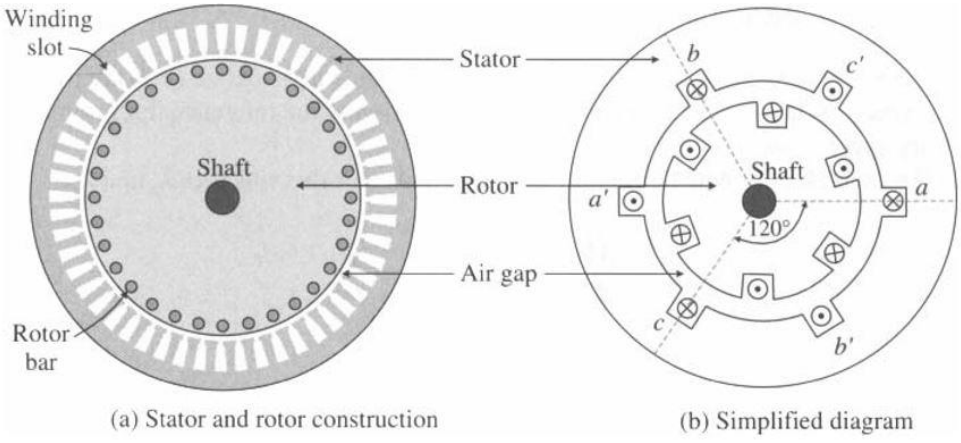

Figure 3-4 Cross-sectional view of a SCIG [9]

There are two generally used dynamic models for the induction generator. One is based on space vector theory, and the other is the dq-axis model derived from the space vector model. The space vector model presents compact mathematical expressions and a single equivalent circuit. However, it requires

complex (real and imaginary part) variables, whereas the dq-frame model is composed of two equivalent circuits, one for each axis. These models are closely related to one another. Moreover, These are equally valid for the analysis of the transient and steady-state performance of the induction generator. In the following sections, both models are presented, and their relationship is explained.

3.3.1 Space-Vector Model

In developing the IG space-vector model, it is assumed:

1. The induction generator is symmetrical in structure and three-phase balanced
2. The magnetic core of the stator and rotor is linear with negligible core losses

The IG space-vector model is usually composed of three sets of equations: voltage equations, flux linkage equations, and motion equation [25],[24]. The voltage equations for the stator and rotor of the generator in the arbitrary reference frame are given by

$$\begin{cases} \vec{v}_s = R_s\vec{i}_s + p\vec{\lambda}_s + j\omega\vec{\lambda}_s \\ \vec{v}_r = R_r\vec{i}_r + p\vec{\lambda}_r + j(\omega - \omega_r)\vec{\lambda}_r \end{cases} \tag{3.13}$$

where

$\vec{v}_s, \vec{v}_r$ - stator and rotor voltage vectors (V)

$\vec{i}_s, \vec{i}_r$ - stator and rotor current vectors (A)

$\vec{\lambda}_s, \vec{\lambda}_r$ - stator and rotor flux-linkage vectors (Wb)

R_s, R_r - stator and rotor winding resistances (Ω)

ω - rotating speed of the arbitrary reference frame (rad/s)

ω_r - rotor electrical angular speed (rad/s)

p - derivative operator $\left(p = \frac{d}{dt}\right)$.

The terms $j\omega\vec{\lambda}_s$ and $j(\omega - \omega_r)\vec{\lambda}_r$ on the right-hand side of Equation (3.13) are referred to as speed voltages. These voltages are induced by the rotation of the reference frame at the arbitrary speed of ω.

The second set of equations is for the stator and rotor flux linkages $\vec{\lambda}_s$ and $\vec{\lambda}_r$:

$$\begin{cases} \vec{\lambda}_s = (L_{ls} + L_m)\vec{i}_s + L_m\,\vec{i}_r = L_s\vec{i}_s + L_m\,\vec{i}_r \\ \vec{\lambda}_r = (L_{lr} + L_m)\vec{i}_r + L_m\,\vec{i}_s = L_r\vec{i}_r + L_m\,\vec{i}_s \end{cases} \tag{3.14}$$

where

$L_s = L_{ls} + L_m$ - stator self-inductance (H)

$L_r = L_{lr} + L_m$ - rotor self-inductance (H)

L_{ls}, L_{lr} - stator and rotor leakage inductances (H)

L_m - magnetizing inductance (H)

Rotor-side parameters and variables, such as $R_r, L_{lr}, \vec{i}_r,$ and $\vec{\lambda}_r$, in Equations (3.13) and (3.14) are referred to the stator side.

The third and final equation is the motion equation, which describes the dynamic behavior of the rotor mechanical speed regarding mechanical and electromagnetic torque:

$$\begin{cases} J\dfrac{d\omega_m}{dt} = T_e - T_m \\ T_e = \dfrac{3P}{2}\mathrm{Re}\left(j\vec{\lambda}_s\vec{i}_s^{*}\right) = -\dfrac{3P}{2}\mathrm{Re}\left(j\vec{\lambda}_r\vec{i}_r^{*}\right) \end{cases} \tag{3.15}$$

where

J - moment of inertia of the rotor (kgm^2)

P - number of pole pairs

T_m - mechanical torque from the generator shaft (N·m)

T_e - electromagnetic torque (N·m)

ω_m - rotor mechanical speed, $\omega_m = \omega_r/P$ (rad/sec)

The above equations constitute the space-vector model of the induction generator, whose equivalent circuit representation is given in Figure 3-5. The generator model is in the arbitrary reference frame, rotating in space at the arbitrary speed ω.

It is vital to note that the IG space-vector model of Figure 3-5 is based on the motor convention. Also, the stator current flows into the stator. This convention is broadly accepted since most induction

machines are used as motors. However, there is no loss of generalization; the space-vector model and its associated equations can be used to model the induction machine either as a motor or a generator.

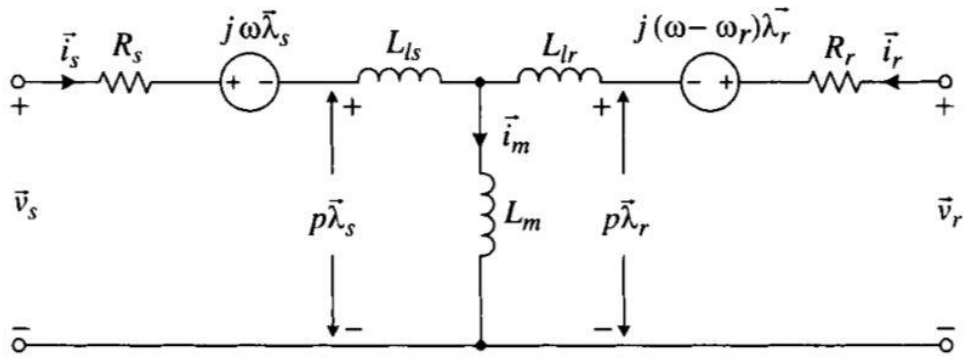

Figure 3-5 Space-vector equivalent circuit of an IG in the arbitrary reference [9]

The induction generator model of Figure 3-5 in the arbitrary reference frame can be directly transformed into the other reference frames. For example, a synchronous frame model is very beneficial for simulation and digital implementation of IG WECS with advanced control systems. Such a model can be found by setting the arbitrary speed ω in Equation (3.13) and in Figure 3-5 to the synchronous speed ω_s. The derived model in the synchronous frame is given in Figure 3-6a, where ω_s is the synchronous speed and ω_{sl} is the angular slip frequency of the generator, given by

$$\begin{cases} \omega_s = 2\pi f_s \\ \omega_{sl} = \omega_s - \omega_r \end{cases} \tag{3.16}$$

The synchronous speed of the reference frame ω_s corresponds to the stator angular frequency, which is proportional to the stator frequency f_s.

To obtain the IG model in the stationary reference frame, we can set the speed of the arbitrary frame ω in Figure 3-5 to zero since the stationary frame does not rotate in space. The resultant equivalent circuit is shown in Figure 3-6b. The IG space-vector models in Figure 3-5 and Figure 3-6 are valid for both SCIG and DFIG. In the SCIG, the rotor circuit is shorted and, therefore, the rotor voltage is set to zero.

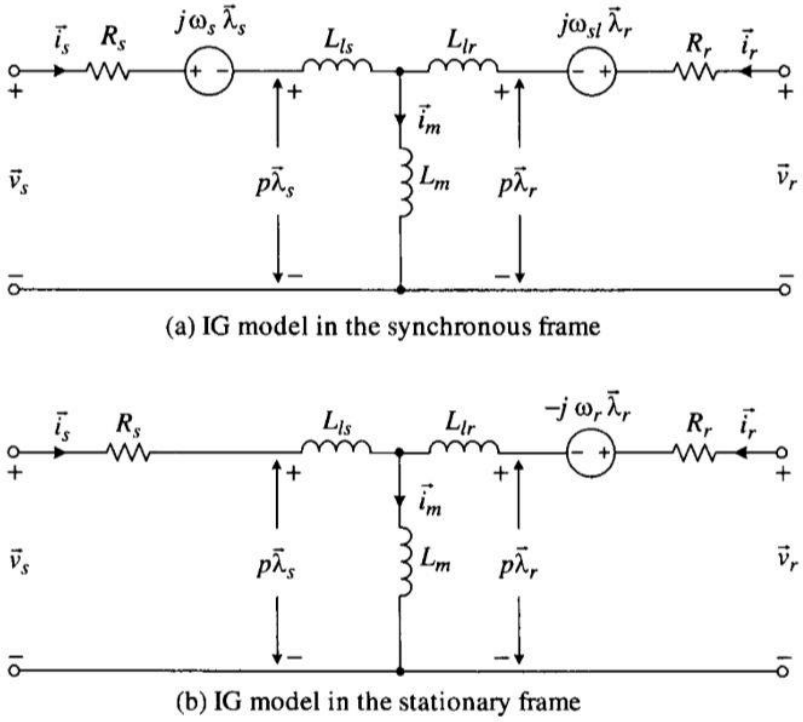

Figure 3-6 Space-vector models for IG in the synchronous and stationary reference frames [9]

3.3.2 dq Reference Frame Model

According to [26], The dq-axis model of the induction generator can be obtained by decomposing the space-vectors into their corresponding d- and q-axis components, that is,

$$\begin{cases} \vec{v}_s = v_{ds} + jv_{qs};\ \vec{i}_s = i_{ds} + ji_{qs};\ \vec{\lambda}_s = \lambda_{ds} + j\lambda_{qs} \\ \vec{v}_r = v_{dr} + jv_{qr};\ \vec{i}_r = i_{dr} + ji_{qr};\ \vec{\lambda}_r = \lambda_{dr} + j\lambda_{qr} \end{cases} \tag{3.17}$$

Substituting Equation (3.17) into Equation (3.13) and grouping real and imaginary components on both sides of the equations, the dq-axis voltage equations for the induction generator are obtained:

$$\begin{cases} v_{ds} = R_s i_{ds} + p\lambda_{ds} - \omega\lambda_{qs} \\ v_{qs} = R_s i_{qs} + p\lambda_{qs} + \omega\lambda_{ds} \\ v_{dr} = R_r i_{dr} + p\lambda_{dr} - (\omega - \omega_r)\lambda_{qr} \\ v_{qr} = R_r i_{qr} + p\lambda_{qr} + (\omega - \omega_r)\lambda_{dr} \end{cases} \tag{3.18}$$

Similarly, substituting Equation (3.17) into Equation (3.14), the dq-axis flux linkages are obtained:

$$\begin{cases} \lambda_{ds} = (L_{ls} + L_m)i_{ds} + L_m i_{dr} = L_s i_{ds} + L_m i_{dr} \\ \lambda_{qs} = (L_{ls} + L_m)i_{qs} + L_m i_{qr} = L_s i_{qs} + L_m i_{qr} \\ \lambda_{dr} = (L_{lr} + L_m)i_{dr} + L_m i_{ds} = L_r i_{dr} + L_m i_{ds} \\ \lambda_{qr} = (L_{lr} + L_m)i_{qr} + L_m i_{qs} = L_r i_{qr} + L_m i_{qs} \end{cases} \tag{3.19}$$

The electromagnetic torque T_e in Equation (3.15) can be expressed by dq-axis flux linkages and currents as well. By mathematical manipulations, several expressions for the torque can be attained. The most commonly used expressions are given by

$$T_e = \begin{cases} \frac{3P}{2}\left(i_{qs}\lambda_{ds} - i_{ds}\lambda_{qs}\right) & (a) \\ \frac{3PL_m}{2}\left(i_{qs}\lambda_{dr} - i_{ds}\lambda_{qr}\right) & (b) \\ \frac{3PL_m}{2L_r}\left(i_{qs}\lambda_{dr} - i_{ds}\lambda_{qr}\right) & (c) \end{cases} \tag{3.20}$$

Equations (3.18) - (3.20) together with the motion equation (3.15) represent the dq-axis model of the induction generator in the arbitrary reference frame, and its corresponding dq-axis equivalent circuits are shown in Figure 3-7 [27], [28]. To obtain the dq-axis model in the synchronous and stationary reference frames, the speed of the arbitrary reference frame ω can be set to the synchronous (stator) frequency ω_s of the generator and zero, respectively.

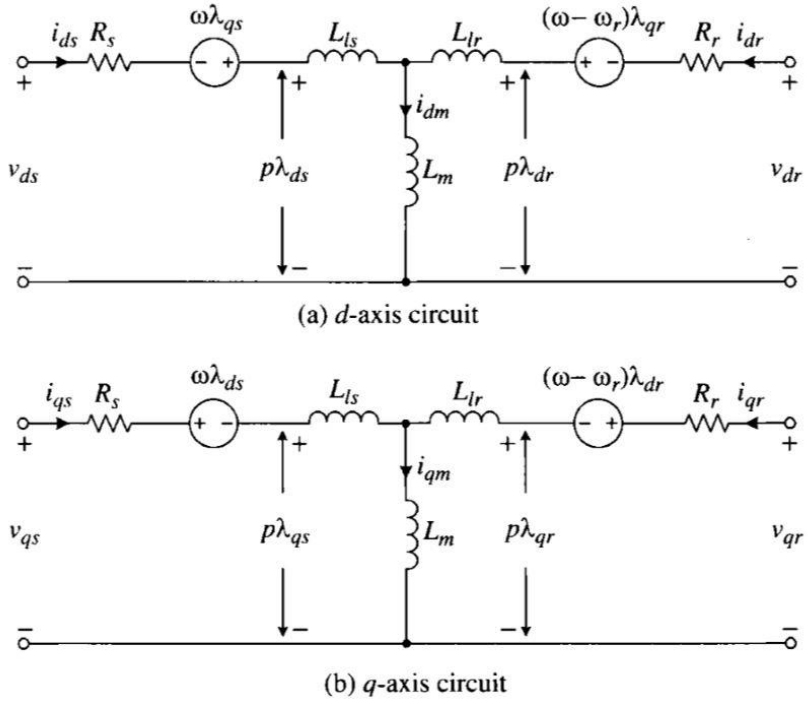

Figure 3-7 IG dq-axis model in the arbitrary reference frame [9]

3.4 Control of SCIG

3.4.1 Field Orientation

The field orientation control can generally be classified into stator flux, air-gap flux, and rotor flux orientations. The rotor flux orientation is simple and easy to implement and is one of the more popular schemes used in both AC drives and wind energy systems [24]. The essence of field-oriented control is the decoupled control of the rotor flux λ_r and electromagnetic torque T_e of the generator to attain high dynamic performance. Using the rotor flux orientation, the stator current of the generator can be decomposed into a flux-producing component, which produces the rotor flux λ_r, and a torque-producing component, which produces the torque T_e. These two components are then controlled independently.

Rotor flux orientation is attained by aligning the d-axis of the synchronous reference frame with the rotor flux vector $\vec{\lambda}_r$, as shown in Figure 3-8. The resultant dq-axis rotor flux components are

$$\begin{cases} \lambda_{qr} = 0 \\ \lambda_{dr} = \sqrt{(\lambda_r)^2 - (\lambda_{qr})^2} = \lambda_r \end{cases} \tag{3.21}$$

where λ_r is the magnitude of $\vec{\lambda}_r$. The rotating speed of the synchronous reference frame is given by

$$\omega_s = 2\pi f_s \tag{3.22}$$

where f_s is the stator frequency of the generator.

Substituting Equation (3.21) into the torque Equation (3.20) yields

$$T_e = K_T \lambda_r i_{qs} \tag{3.23}$$

where $K_T = (3PL_m/3L_r)$. If the rotor flux λ_r is kept constant throughout the generator operation, the q- axis stator current i_{qs} directly controls the developed torque.

The stator current vector $\vec{i}_s$ in Figure 3-8 can be resolved into two components along the dq axes. The d-axis current i_{ds} is the flux-producing current, whereas the q- axis current i_{qs} is the torque-producing current. In field-oriented control, i_{ds} is normally kept at its rated value while i_{qs} is controlled independently. With decoupled control for i_{ds} and i_{qs} , high dynamic performance can be comprehended. It is notable that the stator current vector rotates in space at the synchronous speed. Therefore, i_{ds} and i_{qs} are DC currents in steady state.

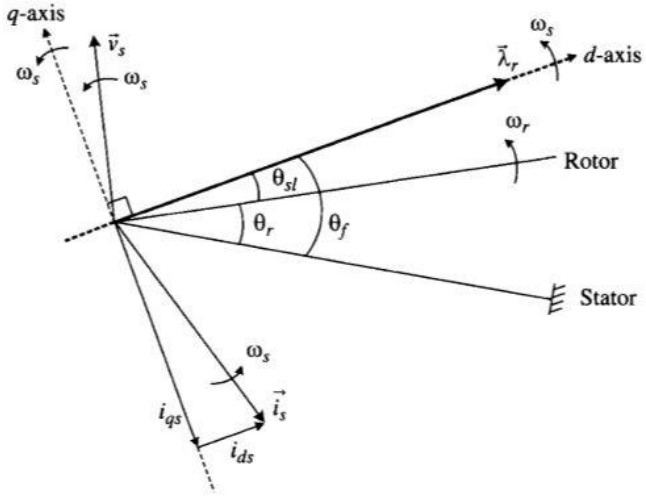

Figure 3-8 Rotor flux-oriented control [24]

One of the key issues linked with the rotor flux-oriented control is to determine accurately the rotor flux angle θ_f for field orientation. Different methods can be used to find θ_f. The method is known as direct field-oriented control if the angle is obtained through the measurement of generator terminal voltages and currents.

3.4.2 Direct field-oriented control

Figure 3-9 shows a typical block diagram of a direct field-oriented control for the induction generator [24], To implement the FOC scheme, the rotor flux magnitude λ_r and its angle θ_f are identified by the rotor flux calculator based on the measured stator voltages (v_{as} and v_{bs}) and currents (i_{as} and i_{bs}).

There are three feedback control loops: one for the rotor flux linkage λ_r, one for the d -axis stator current i_{ds}, and another for the q -axis stator current i_{qs}. For the rotor flux control, the measured λ_r is compared with its reference λ_r^* and the error is passed through a PI controller. The output of the PI regulator yields the d-axis stator current reference i_{ds}^*. The torque reference T_e^* is generated by the maximum power point tracking scheme. The q-axis stator current reference can then be calculated by

$$i_{qs}^* = \frac{T_e^*}{K_T \lambda_r} \tag{3.24}$$

The feedback dq-axis stator currents i_{ds} and i_{qs} are compared with their references, and the errors are sent to current PI controllers to generate stator voltage references v_{ds}^* and v_{qs}^*. The voltages at dq-axis in the synchronous reference frame are then transformed to the three-phase stator voltages v_{as}^*, v_{bs}^*, and v_{cs}^* in the stationary frame through the dq/abc transformation block.

For the space vector modulation, the reference vector, $\vec{v}_{ref}$ is generated according to the three-phase reference voltages v_{as}^*, v_{bs}^*, and v_{cs}^*, based on which the PWM gating signals are produced.

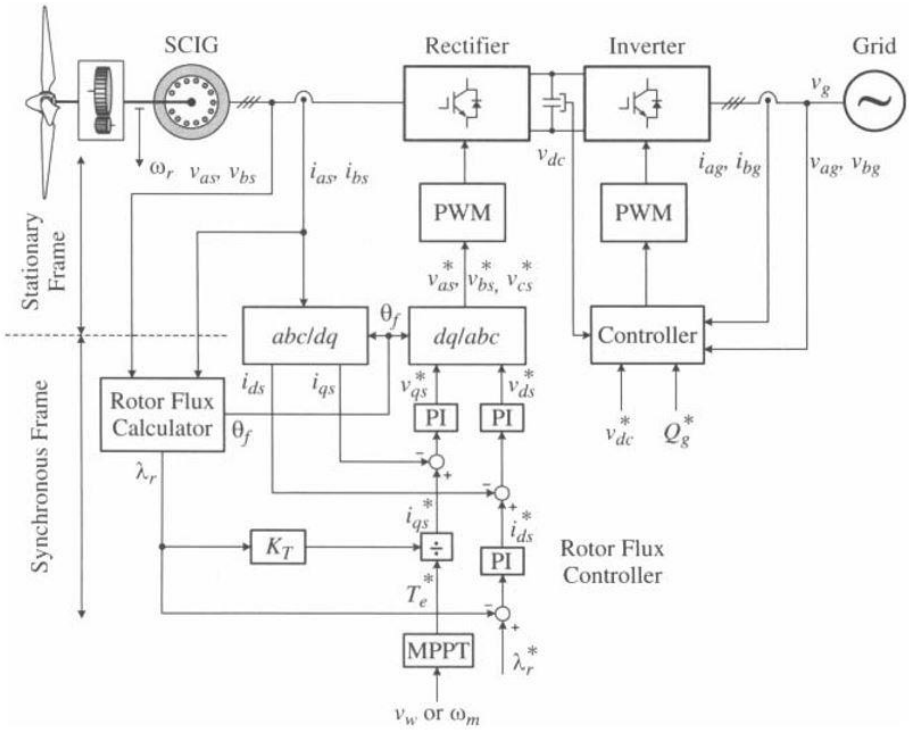

Figure 3-9 Direct field-oriented control with rotor flux orientation [24]

As shown in Figure 3-9, the rotor flux angle θ_f is used in the abc/dq and dq/abc transformation for field orientation. Neglecting switching harmonics produced by the rectifier, the variables above the transformation blocks (as separated in Figure 3-9 by dashed lines on the left side) are all in the stationary reference frame, which are sinusoidal in steady state, whereas the variables below transformation blocks are all DC signals in the rotor flux synchronous frame.

3.4.3 Rotor Flux Calculator

The generator model in the stationary dq-axis frame in Figure 3-10a can be utilized to calculate the rotor flux magnitude and angle. The stator flux vector can be given as

$$\vec{\lambda}_s = \int (\vec{v}_s - R_s \vec{i}_s)\, dt \tag{3.25}$$

The rotor flux vector can be calculated by

$$\vec{\lambda}_r = L_r \vec{i}_r + L_m \vec{i}_s = \frac{\vec{\lambda}_s - L_s \vec{i}_s}{L_m} + L_m \vec{i}_s = \frac{L_r}{L_m}\left(\vec{\lambda}_s - \sigma L_s \vec{i}_s\right) \tag{3.26}$$

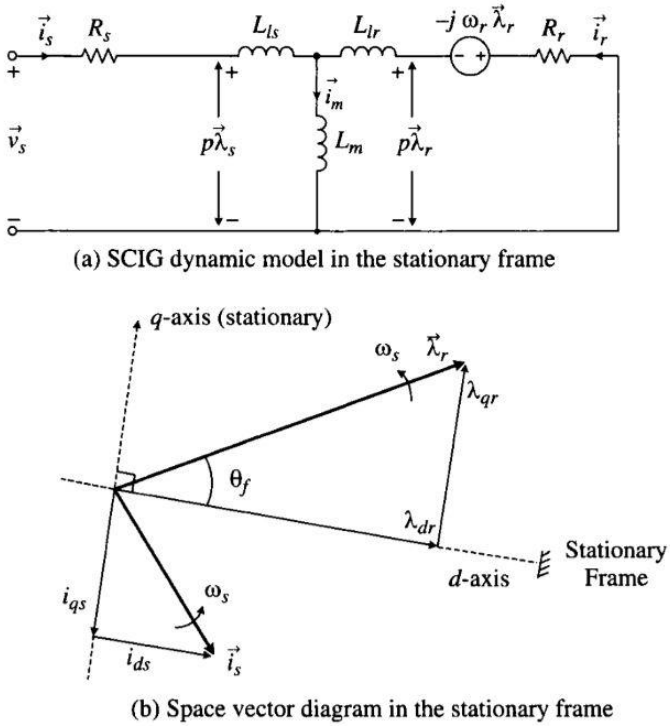

Figure 3-10 Dynamic model of SCIG and space vector diagram for rotor flux calculation [9]

σ in Equation (3.26) is the total leakage factor, defined by

$$\sigma = 1 - \frac{L_m^2}{L_s L_r} \tag{3.27}$$

Decomposing the rotor flux $\vec{\lambda}_r$ into the d- and q-axis components in the stationary frame, we have

$$\begin{cases} \lambda_{dr} = \dfrac{L_r}{L_m}(\lambda_{ds} - \sigma L_s i_{ds}) \\ \lambda_{qr} = \dfrac{L_r}{L_m}(\lambda_{qs} - \sigma L_s i_{qs}) \end{cases} \tag{3.28}$$

from which the magnitude and angle of the rotor flux are

$$\begin{cases} \lambda_r = \sqrt{\lambda_{dr}^2 + \lambda_{qr}^2} \\ \theta_f = \tan^{-1}\dfrac{\lambda_{qr}}{\lambda_{dr}} \end{cases} \tag{3.29}$$

From the above equations that the rotor flux magnitude λ_r and its angle θ_f can be calculated based on measured stator voltage, stator current, and generator parameters ($L_s, L_r, L_m,$ and R_s). No rotor current is required for the calculation. Figure 3-10b shows the vector diagram for the rotor flux vector $\vec{\lambda}_r$ and

stator current vector $\vec{i}_s$ used in the rotor flux calculator. When the two vectors rotate one revolution in space, their dq-axis components, $\lambda_{dr}, \lambda_{qr}, i_{ds}$, and i_{qr}, alter one cycle over time due to the usage of the stationary (stator) frame. Neglecting the switching harmonics, these variables are sinusoidal in steady state.

Figure 3-11 shows the block diagram for the digital implementation of a rotor flux calculator. Of the three stator voltages v_{as}, v_{bs}, and v_{cs} , only two require to be measured and the third can be found from $v_{as} + v_{bs} + v_{cs} = 0$. This statement is applicable for the stator currents also. The stator voltages and currents are then transformed into two-phase variables through $abc/\alpha\beta$ stationary transformation blocks. The other blocks are derived from Equations (3.25) - (3.29). The rotor flux angle θ_f for field orientation and its amplitude λ_r for rotor flux feedback control.

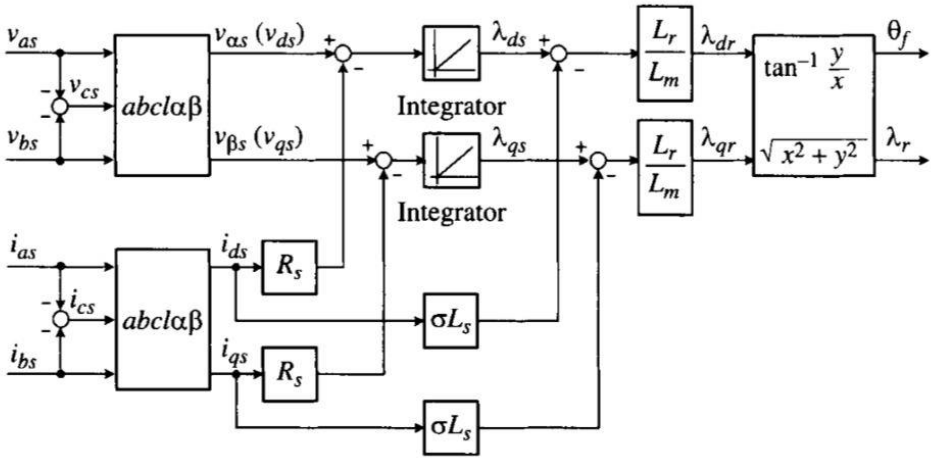

Figure 3-11 Block diagram of a rotor flux calculator [9]

It is considered that the dq-axis voltages and currents in the rotor flux calculator are all AC signals, which may cause problems for the integrators, such as undesired DC offsets during system start-up. In practice, the integrators can be replaced by first-order, low-pass filters with a low cut-off frequency up to a couple of hertz. The replacement of integrators by low-pass filters has little impact on system operation since the wind generator normally operates at much higher stator frequencies than the filter cut off frequency.

4 Converter Modeling

In variable-speed squirrel cage induction generator (SCIG) wind energy conversion systems (WECS), full-capacity power converters i.e. 2L-VSC are required to adjust the speed of the generator in order to harvest the maximum possible power available from the wind. The generator-side converter (rectifier) is used to control the speed or torque of the generator with a maximum power point tracking (MPPT) scheme. The grid-side converter (inverter) is employed for the control of DC link voltage and grid-side reactive power [24].

The main advantages of the 2L-VSC include its simplicity, proven technology and the possibility of building redundancy into the string of series-connected switching devices, usually insulated gate bipolar transistors (IGBTs). The two-level VSC allows the IGBTs to be connected in series, depending on the voltage rating of the device available and the supply voltage required. The fundamental principle of a single-phase, two-level VSC is shown in Figure 4-1, where the output waveform has two levels, $+V_{dc}$ and 0. Therefore, each switch string must be rated for the full direct voltage, V_{dc}. Due to the large capacitance of the DC side of the converter, the DC voltage, V_{dc}, is more or less constant and thus the converter is known as a voltage source converter [29].

Three single-phase, two-level voltage source converters can be connected to the same capacitor to form a three-phase converter. This power converter circuit arrangement is often called the six-pulse converter configuration. In this circuit, the switches in one leg are switched alternatively with a small dead time to avoid both conducting simultaneously. Therefore, one switching function is enough to control both switches in a leg [30].

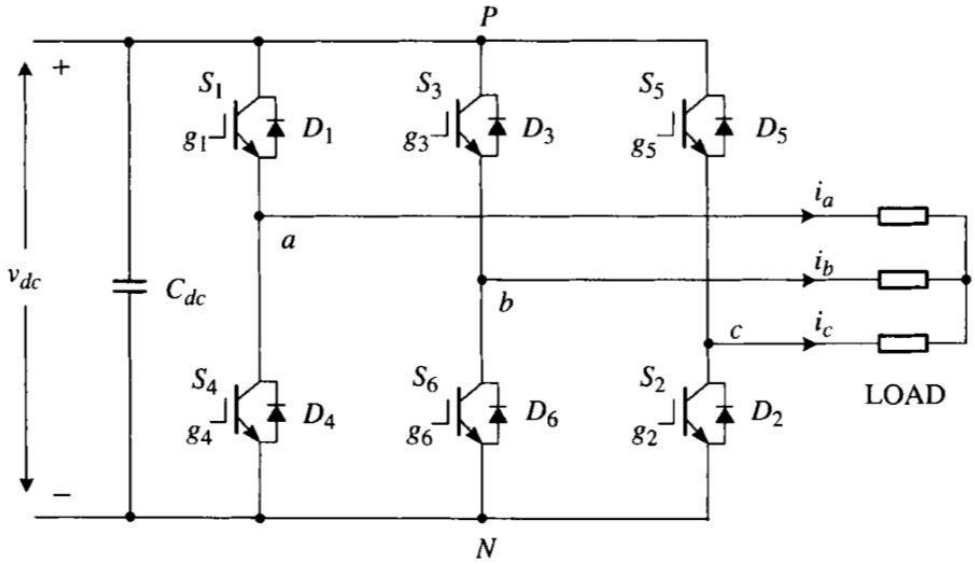

Figure 4-1 Converter topology [9]

There are some different switching strategies for VSCs [30]–[32]. These include square-wave operation, carrier-based pulse-width modulation (CB-PWM) techniques such as switching frequency optimal

PWM (SFO-PWM), sinusoidal regular sampled PWM (RS-PWM), non-regular sampled PWM (NRS-PWM), selective harmonic elimination PWM (SHEM), space vector PWM (SV-PWM) and hysteresis switching techniques. In this case, SV-PWM is selected.

4.1 Space Vector Modulation

Space vector modulation (SVM) is one of the real-time modulation techniques and is widely used for digital control of voltage source inverters [24].

Switching States

The performing status of the switches in the 2 - level inverter in Figure 4-1 can be represented by switching states. As indicated in Table 4-1, switching state P denotes that the upper switch in a converter leg is on and the converter terminal voltage (v_{aN}, v_{bN}, or v_{cN}) is positive ($+V_{dc}$), whereas O indicates that the converter terminal voltage is zero due to the conduction of the lower switch.

Table 4-1 Definition of switching states [24]

Switching states	Leg a			Leg b			Leg c		
	S_1	S_4	v_{aN}	S_3	S_6	v_{bN}	S_5	S_2	v_{cN}
P	On	Off	V_{dc}	On	Off	V_{dc}	On	Off	V_{dc}
O	Off	On	0	Off	On	0	Off	On	0

There are eight possible combinations of switching states in the 2-level inverter as listed in Table 4-2. The switching state [POO], for example, corresponds to the conduction of S_1, S_6, and S_2 in the inverter legs a, b, and c, respectively. Among the eight switching states, [PPP] and [OOO] are zero states and the others are active states.

Space Vectors

The active and zero switching states can be represented by active and zero space vectors, respectively. A typical space vector diagram for the two-level inverter is shown in Figure 4-2, where the six active vectors $\vec{V}_1$ to $\vec{V}_6$ form a regular hexagon with six equal sectors (I to VI). The zero vector $\vec{V}_0$ lies at the centre of the hexagon.

Table 4-2 Space vector, switching states, and on-state switches [24]

Space vector		Switching state (three phases)	On-state switch	Vector definition
Zero vector	$\vec{V}_0$	[PPP] [OOO]	S_1, S_3, S_5 S_4, S_6, S_5	$\vec{V}_0 = 0$
Active vector	$\vec{V}_1$	[POO]	S_1, S_6, S_2	$\vec{V}_1 = \frac{2}{3}V_{dc}e^{j0}$
	$\vec{V}_2$	[PPO]	S_1, S_3, S_2	$\vec{V}_2 = \frac{2}{3}V_{dc}e^{j\frac{\pi}{3}}$
	$\vec{V}_3$	[OPO]	S_4, S_3, S_2	$\vec{V}_3 = \frac{2}{3}V_{dc}e^{j\frac{2\pi}{3}}$
	$\vec{V}_4$	[OPP]	S_4, S_3, S_5	$\vec{V}_4 = \frac{2}{3}V_{dc}e^{j\frac{3\pi}{3}}$
	$\vec{V}_5$	[OOP]	S_4, S_6, S_5	$\vec{V}_5 = \frac{2}{3}V_{dc}e^{j\frac{4\pi}{3}}$
	$\vec{V}_6$	[POP]	S_1, S_6, S_5	$\vec{V}_6 = \frac{2}{3}V_{dc}e^{j\frac{5\pi}{3}}$

To derive the relationship between the space vectors and switching states, refer to the 2-level inverter in Figure 4-1. Assuming that the operation of the inverter is 3-phase balanced, we have

$$v_a(t) + v_b(t) + v_c(t) = 0 \tag{4.1}$$

Where v_a, v_b and v_c are the instantaneous load phase voltages. From a mathematical point of view, one of the phase voltages is redundant since, given any two-phase voltages, the third one can be readily calculated. Therefore, it is possible to transform the three-phase variables to two-phase variables through the abc/αβ transformation.

$$\begin{bmatrix} v_\alpha(t) \\ v_\beta(t) \end{bmatrix} = \frac{2}{3}\begin{bmatrix} 1 & -\frac{1}{2} & -\frac{1}{2} \\ 0 & \frac{\sqrt{3}}{2} & -\frac{\sqrt{3}}{2} \end{bmatrix} \cdot \begin{bmatrix} v_a(t) \\ v_b(t) \\ v_c(t) \end{bmatrix} \tag{4.2}$$

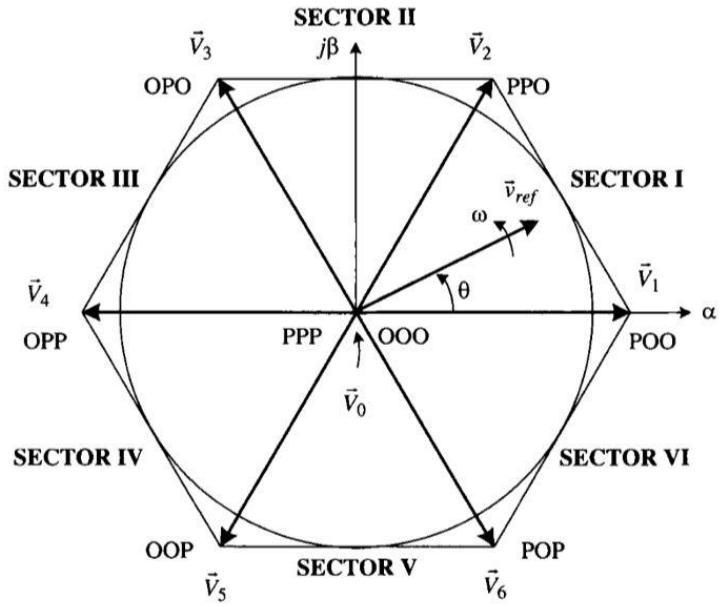

Figure 4-2 Space-vector diagram for the two-level inverter [24]

A space vector can generally be expressed regarding the two-phase voltages in the αβ frame:

$$\vec{v}(t) = v_\alpha(t) + v_\beta(t) \tag{4.3}$$

Substituting (4.2) into (4.3),

$$\vec{v}(t) = \frac{2}{3}\left[v_a(t)e^{j0} + v_b(t)e^{j2\pi/3} + v_c(t)e^{j4\pi/3}\right] \tag{4.4}$$

where $e^{jx} = \cos x + \sin x$ and $x = 0, 2\pi/3$ or $4\pi/3$. For the active switching state [POO], the generated load phase voltages are

$$v_a(t) = \frac{2}{3}V_{dc}, v_b(t) = -\frac{1}{3}V_{dc}, \text{and}, v_c(t) = -\frac{1}{3}V_{dc} \tag{4.5}$$

The corresponding space vector denoted as $\vec{V}_1$ can be obtained by substituting (4.5) into (4.4):

$$V_1 = \frac{2}{3}V_{dc}e^{j0} \tag{4.6}$$

Following the same procedure, all six active vectors can be derived:

$$\vec{V}_k = \frac{2}{3}V_{dc}e^{j(k-1)\frac{\pi}{3}} \qquad k = 1,2,\ldots,6 \tag{4.7}$$

The zero vector $\vec{V}_0$ has two switching states [PPP] and [OOO], one of which is redundant. As will be seen later, the redundant switching state can be utilized to minimize the switching frequency of the inverter or perform other useful functions. The relationship between the space vectors and their corresponding switching states is given in Table 4-2.

It is noted that the zero and active vectors do not move in space and, thus, are referred to as stationary vectors. On the contrary, the reference vector $\vec{v}_{ref}$ in Figure 4-2 rotates in space at an angular velocity

$$\omega_s = 2\pi f \tag{4.8}$$

Where f is the fundamental frequency of the inverter output voltage. The angular displacement between $\vec{v}_{ref}$ and the α-axis of the $\alpha - \beta$ frame can be obtained by

$$\theta(t) = \int_0^t \omega_s(t)dt + \theta_0 \tag{4.9}$$

For a given magnitude and position, $\vec{v}_{ref}$ can be synthesized by three nearby stationary vectors, based on which the switching states of the inverter can be selected, and gate signals for the active switches can be generated. When $\vec{v}_{ref}$ passes through the sectors one by one, different sets of switches will be turned on or off. As a result, when $\vec{v}_{ref}$ revolves one revolution in space; the inverter output voltage varies one cycle over time. The inverter output frequency corresponds to the rotating speed of $\vec{v}_{ref}$, whereas its output voltage can be adjusted by the magnitude of $\vec{v}_{ref}$.

Dwell Time Calculation

As mentioned earlier, the reference $\vec{v}_{ref}$ can be synthesized by three stationary vectors. The dwell time for the stationary vectors basically represents the duty-cycle time (on-state or off-state time) of the chosen switches during a sampling period T_s. The dwell time calculation is based on the volt-second balancing principle, that is, the multiplication of the reference voltage $\vec{v}_{ref}$ and sampling period T_s equals the sum of the voltage multiplied by the time interval of selected space vectors.

Assuming that the sampling period T_s is sufficiently small, the reference vector $\vec{v}_{ref}$ can be considered constant during T_s. Under this assumption, $\vec{v}_{ref}$ can be approximated by two adjacent active vectors and one zero vector. For example, when $\vec{v}_{ref}$ falls into sector I, as shown in Figure 4-3, it can be synthesized by $\vec{V}_1$, $\vec{V}_2$ and $\vec{V}_0$. The volt-second balancing equation is

$$\begin{cases} \vec{v}_{ref} T_s = \vec{V}_1 T_a + \vec{V}_2 T_b + \vec{V}_0 T_0 \\ T_s = T_a + T_b + T_0 \end{cases} \tag{4.10}$$

where $T_a, T_b,$ and T_0 are the dwell times for the vectors $\vec{V}_1$, $\vec{V}_2$ and $\vec{V}_0$, respectively. The space vectors in Equation (4.7) can be expressed as

$$\vec{v}_{ref} = v_{ref}\, e^{j\theta}, \vec{V}_1 = \frac{2}{3}V_{dc}, \vec{V}_2 = \frac{2}{3}V_{dc}\, e^{j\frac{\pi}{3}}, \text{and } \vec{V}_0 = 0 \tag{4.11}$$

Where v_{ref} shows the magnitude of the reference vector and θ is the angle between v_{ref}. The α-axis of the $\alpha - \beta$ frame as shown in Figure 4-2.

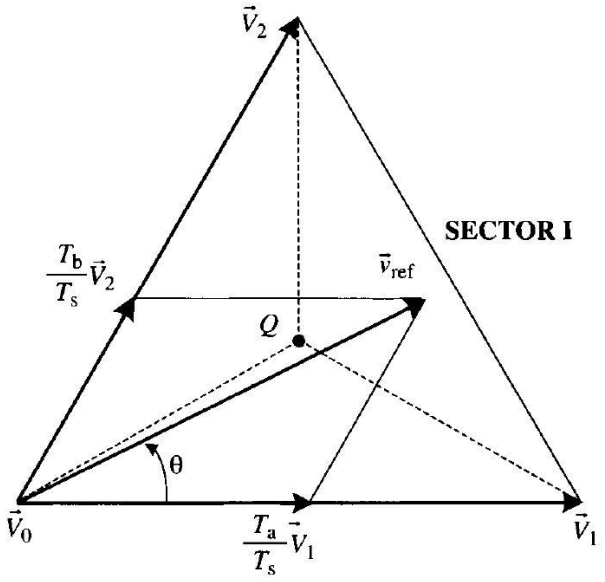

Figure 4-3 Reference voltage synthesized by 3-phase voltages vector [24]

Substituting (4.11) into (4.10) and then splitting the resultant equation into the real (α-axis) and imaginary (β-axis) components in the $\alpha - \beta$ frame,

$$\begin{cases} \text{Re: } v_{ref}(\cos\theta)T_s = \frac{2}{3}V_{dc}T_a + \frac{1}{3}V_{dc}T_b \\ \text{Im: } v_{ref}(\sin\theta)T_s = \frac{1}{\sqrt{3}}V_{dc}T_b \end{cases} \tag{4.12}$$

Solving (4.12) together with $T_s = T_a + T_b + T_0$ yields

$$\begin{cases} T_a = \frac{\sqrt{3}\,T_s\, v_{ref}}{V_{dc}}\sin\left(\frac{\pi}{3} - \theta\right) \\ T_b = \frac{\sqrt{3}\,T_s\, v_{ref}}{V_{dc}}\sin\theta \qquad \text{for } 0 \le \theta < \pi/3 \\ T_0 = T_s - T_a - T_b \end{cases} \tag{4.13}$$

To anticipate the relationship between the location of $\vec{v}_{ref}$ and the dwell times, by examining some special cases. If $\vec{v}_{ref}$ lies precisely in the middle between $\vec{V}_1$ and $\vec{V}_2$ (i.e., $\theta = \pi/6$), the dwell time T_a of $\vec{V}_1$ will be equal to T_b of $\vec{V}_2$. When $\vec{v}_{ref}$ is closer to $\vec{V}_2$, T_b will be greater than T_a. If $\vec{v}_{ref}$ is coincident with

$\vec{V}_2$, T_a will be zero. With the head of $\vec{v}_{ref}$ located right on the central point Q, $T_a = T_b = T_0$. The relationship between the $\vec{v}_{ref}$ location and dwell times is summarized in Table 4-3.

Note that although Equation (4.13) is derived when $\vec{v}_{ref}$ is in the sector I; it can also be used when $\vec{v}_{ref}$ is in other sectors, providing that a multiple of $\pi/3$ is subtracted from the actual angular displacement θ such that the modified angle θ' falls into the range between zero and $\pi/3$ for use in the equation, that is,

$$\theta' = \theta - (k-1)\,\pi/3 \qquad \text{for } 0 \le \theta' < \pi/3 \tag{4.14}$$

where k = 1, 2..., 6 for sectors I, II..., VI, respectively. For example, when $\vec{v}_{ref}$ is in sector II, the calculated dwell times $T_a, T_b,$ and T_0 based on Equation (4.13) are for vectors $\vec{V}_1$, $\vec{V}_2$ and $\vec{V}_0$, respectively.

Table 4-3 Reference voltage location and dwell times [9]

$\vec{v}_{ref}$ Location	$\theta = 0$	$0 < \theta < \frac{\pi}{6}$	$\theta = \frac{\pi}{6}$	$\frac{\pi}{6} < \theta < \frac{\pi}{3}$	$\theta = \frac{\pi}{3}$
Dwell times	$T_a > 0$ $T_b = 0$	$T_a > T_b$	$T_a = T_b$	$T_a < T_b$	$T_a = 0$ $T_b > 0$

Modulation Index

Equation (4.13) can also be expressed regarding modulation index m_a:

$$\begin{cases} T_a = T_s m_a \sin\left(\frac{\pi}{3} - \theta\right) \\ T_b = T_s m_a \sin\theta \\ T_0 = T_s - T_a - T_b \end{cases} \qquad \text{for } 0 \le \theta < \pi/3 \tag{4.15}$$

where

$$m_a = \frac{\sqrt{3} v_{ref}}{V_{dc}} \tag{4.16}$$

The length of the reference vector $\vec{v}_{ref}$ represents the peak value of the fundamental-frequency component in the inverter output phase voltage, that is,

$$v_{ref} = \hat{V}_{a1} = \sqrt{2} V_{a1} \tag{4.17}$$

Where V_{a1} is the rms value of the fundamental component in the inverter output phase (phase-a) voltage. Substituting (4.17) into (4.16), the relationship between m_a and V_{a1} can be found:

$$m_a = \frac{\sqrt{3}v_{ref}}{V_{dc}} = \frac{\sqrt{6}V_{a1}}{V_{dc}} \tag{4.18}$$

For a given DC voltage V_{dc}, the inverter output voltage V_{a1} is proportional to the modulation index m_a.

The maximum length of the reference vector, $v_{ref,max}$, corelates to the radius of the largest circle that can be inscribed within the hexagon, as shown in Figure 4-2. Since the hexagon is formed by six active vectors having a length of $2V_{dc}/3$, $v_{ref,max}$ can be found from

$$v_{ref,max} = \frac{2}{3}V_{dc}.\frac{\sqrt{3}}{2} = \frac{V_{dc}}{\sqrt{3}} \tag{4.19}$$

Substituting (4.19) into (4.16) gives the maximum modulation index

$$m_a = 1 \tag{4.20}$$

from which the modulation index for the space vector modulation scheme is in the range of

$$0 \leq m_a \leq 1 \tag{4.21}$$

Switching Sequence

With the space vectors selected and their dwell times calculated, the next step is to arrange the switching sequence. In general, the switching sequence design for a given $\vec{v}_{ref}$ is not unique, but it should satisfy the following two requirements to minimize device switching frequency:

1. The changeover from one switching state to the next contains only two switches in the same inverter leg, one being switched on and the other switched off.
2. The transition for $\vec{v}_{ref}$ moving from one sector in the space vector diagram to the next requires no or a minimum number of switching.

Figure 4-4 shows a typical seven-segment switching sequence and inverter output voltage waveforms for $\vec{v}_{ref}$ in the sector I, where $\vec{v}_{ref}$ is synthesized by $\vec{V}_1$, $\vec{V}_2$ and $\vec{V}_0$. The sampling period T_s is separated into seven segments for the selected vectors. It can be realized that

- The dwell times for the seven segments add up to the sampling period ($T_s = T_a + T_b + T_0$).

- Design requirement (1) is fulfilled. For instance, the transition from [OOO] to [POO] is accomplished by turning S_1, on and S_4 off, which involves only two switches.
- The redundant switching states for $\vec{V}_0$ are utilized to reduce the number of switching per sampling period. For the $T_0/2$ the segment in the center of the sampling period, the switching state [PPP] is selected, whereas for the $T_0/4$ segments on both sides, the state [OOO] is used.
- Each of the switches in the inverter turns on and off once per sampling period. The switching frequency f_{sw} of the devices is thus equal to the sampling frequency f_{sp}, that is, $f_{sw} = f_{sp} = 1/T_s$.

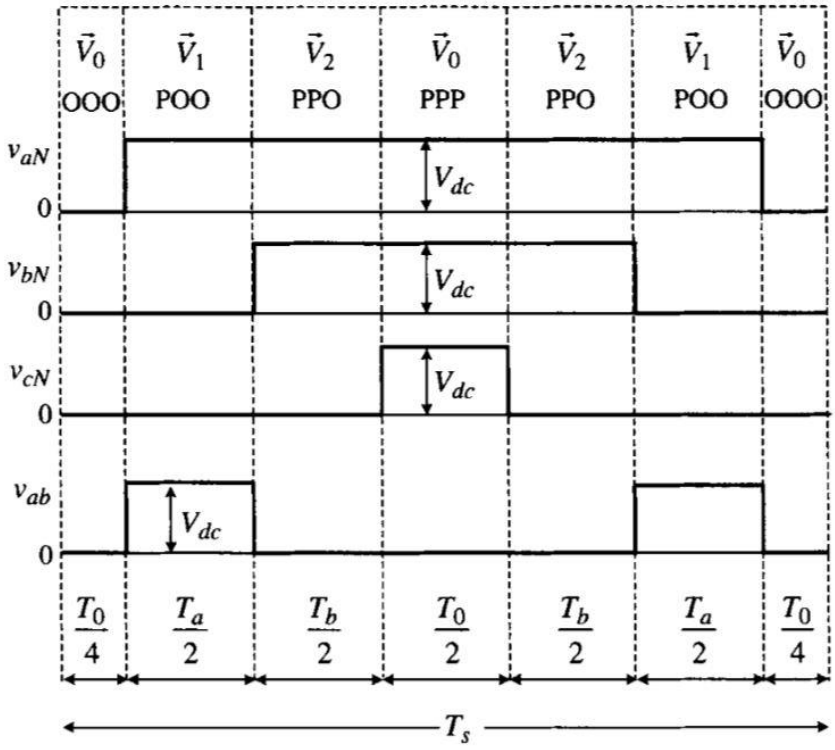

Figure 4-4 Seven-segment switching sequence for reference voltage in sector I [24]

The two-level voltage source converter technology is broadly accepted in the variable-speed WECS, including squirrel cage induction generator (SCIG), doubly fed induction generator (DFIG), and synchronous generator (SG) based WES. The converter can be utilized either as a rectifier that converts three-phase AC voltage produced by the generator to a DC voltage or as a grid-connected inverter that delivers the active power from the generator and rectifier to the grid.

4.2 Control of Grid-Connected Inverter

Most commercial wind turbines deliver the generated power to the electric grid through power converters. A typical grid-connected inverter for wind energy applications is shown in Figure 4-5, where a two-level voltage source inverter is used. The inverter is connected to the grid through a line inductance L_g, which represents the leakage inductance of the transformer, if any, and the line reactor of 0.05 to 0.1 per unit, which usually is added to the system for the reduction of line current distortion. The line resistance is negligibly small and has little impact on the system performance [24],[33].

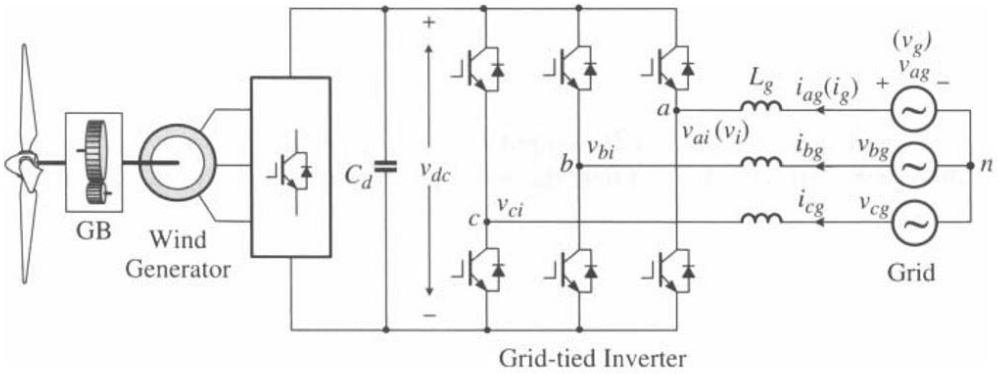

Figure 4-5 Grid-connected inverter in a wind energy system [9]

The space vector modulation scheme modulates the grid-tied inverter. The inverter is a boost converter by nature and its average DC voltage V_{dc} can be derived from Equation (4.18) and given by

$$V_{dc} = \frac{\sqrt{6}V_{ai1}}{m_a} \qquad \text{for } 0 < m_a \leq 1 \tag{4.22}$$

where m_a is the modulation index and V_{ai1} is the rms value of the fundamental-frequency component of the inverter phase (phase-a) voltage V_{ai1}. Assuming that $V_{ai1}$is equal to the rms value of grid phase voltage V_g, which can be considered constant, the DC voltage can be boosted to a high value by a small m_a.

Figure 4-6a shows a simplified diagram for a wind energy system, in which the wind turbine, generator, and rectifier are replaced by a battery in series with a small resistance that represents the power losses in the system. The power flow between the inverter and grid is bidirectional. Power can be transferred from the grid to the DC circuit of the inverter, or vice versa. For wind energy applications, the power is generally delivered to the grid from the inverter. The active power of the system delivered to the grid can be calculated by

$$P_g = 3\,V_g I_g \cos\varphi_g \tag{4.23}$$

where φ_g is the grid power factor angle, defined by

$$\varphi_g = \angle\bar{V}_g - \angle\bar{I}_g \tag{4.24}$$

The grid power factor can be unity, leading, or lagging, as shown in Figure 4-6b. The TSOs often require that a wind energy system offer controllable reactive power to the grid to support the grid voltage in addition to the active power production. Therefore, a wind energy system can operate with the power factor angle in the range of $90° \leq \varphi_g < 270°$.

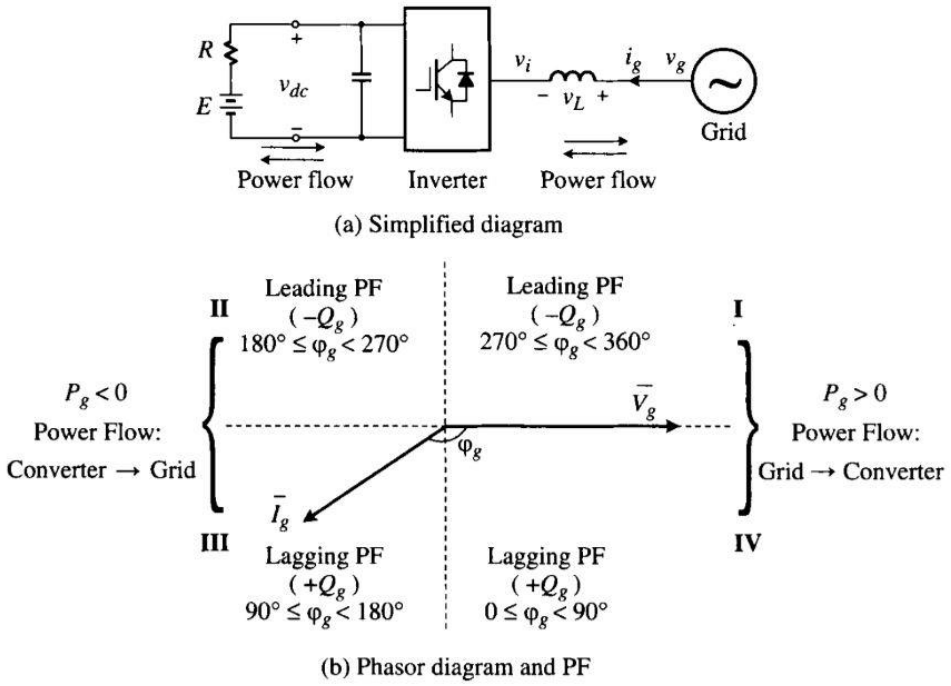

Figure 4-6 Simplified system diagram and definition of power factor [9]

4.2.1 Voltage Oriented Control (VOC)

The grid-connected inverter can be controlled with many schemes. One of the schemes is known as voltage-oriented control (VOC), as shown in Figure 4-7. This scheme is based on transformation between the abc stationary reference frame and dq synchronous frame. The control algorithm is implemented in the grid-voltage synchronous reference frame, where all the variables are of DC components in steady state. This simplifies the design and control of the inverter.

To understand the VOC, the grid voltage is measured and its angle θ_g is detected the voltage orientation. This angle is used for the transformation of variables from the abc stationary frame to the dq

synchronous frame through the abc/dq transformation or from the synchronous frame back to the stationary frame through the dq/abc transformation, as shown in Figure 4-7. Several methods are available to detect the grid voltage angle θ_g. Assuming that the grid voltages, $v_{ag}, v_{bg}, \text{and } v_{cg}$, are three-phase balanced sinusoidal waveforms, θ_g can be obtained by

$$\theta_g = \tan^{-1}\frac{v_\beta}{v_\alpha} \tag{4.25}$$

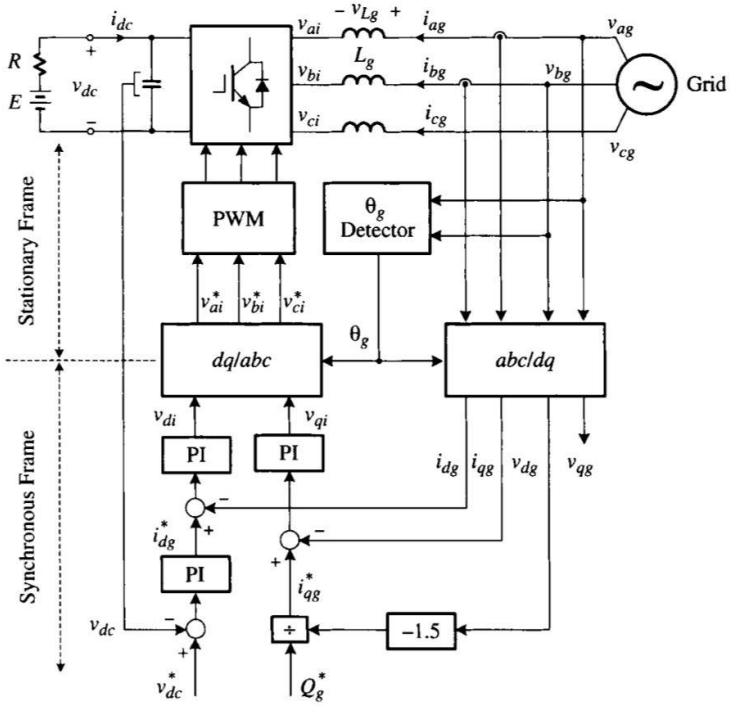

Figure 4-7 Block diagram of voltage-oriented control (VOC) [9]

where v_α and v_β can be obtained by the $abc/\alpha\beta$ transformation:

$$\begin{cases} v_\alpha = \frac{2}{3}\left(v_{ag} - \frac{1}{2}v_{bg} - \frac{1}{2}v_{cg}\right) = v_{ag} \\ v_\beta = \frac{2}{3}\left(\frac{\sqrt{3}}{2}v_{bg} - \frac{\sqrt{3}}{2}v_{cg}\right) = \frac{\sqrt{3}}{3}\left(v_{ag} + 2v_{bg}\right) \end{cases} \quad \text{for } v_{ag} + v_{bg} + v_{cg} = 0 \tag{4.26}$$

Equation (4.26) indicates that there is no need to measure the phase-c grid voltage v_{cg} as shown in Figure 4-7. In reality, the grid voltage may contain harmonics and be distorted, so digital filters or phase-locked loops (PLLs) may be used for the detection of the grid voltage angle θ_g. There are three feedback control loops in the system: two inner current loops for the accurate control of the dq-axis currents i_{dg} and i_{qg}, and one outer DC voltage feedback loop for the control of DC voltage v_{dc}. With the VOC

scheme, the three-phase line currents in the abc stationary frame $i_{ag}, i_{bg}, \text{and } i_{cg}$ are transformed to the two-phase currents i_{dg} and i_{qg} in the dq synchronous frame, which are the active and reactive components of the three-phase line currents, respectively. The independent control of these two components offers an effective means for the independent control of active and reactive power of the system.

To achieve the VOC control scheme, the d-axis of the synchronous frame is aligned with the grid voltage vector. Therefore the d-axis grid voltage is equal to its magnitude $(v_{dg} = v_g)$, moreover, the resultant q-axis voltage v_{qg} is then equal to zero $\left(v_{qg} = \sqrt{v_g^2 - v_{dg}^2} = 0\right)$, from which the active and reactive power of the system can be calculated by

$$\begin{cases} P_g = \dfrac{3}{2}\left(v_{dg}i_{dg} + v_{qg}i_{qg}\right) = \dfrac{3}{2}v_{dg}i_{dg} \\ Q_g = \dfrac{3}{2}\left(v_{qg}i_{dg} - v_{dg}i_{qg}\right) = -\dfrac{3}{2}v_{dg}i_{qg} \end{cases} \quad \text{for } v_{qg} = 0 \qquad (4.27)$$

The q-axis current reference i_{qg}^* can then be obtained from

$$i_{qg}^* = \frac{Q_g^*}{-1.5v_{dg}} \qquad (4.28)$$

where Q_g^* is the reference for the reactive power, which can be set to zero for unity power factor operation, a negative value for leading power factor operation, or positive value for lagging power factor operation.

The d-axis current reference i_{dg}^*, which characterizes the active power of the system, is generated by the PI controller for DC voltage control. When the inverter operates in steady state, the DC voltage v_{dc} of the inverter is kept constant at a value set by its reference voltage v_{dc}^*. The PI controller generates the reference current i_{dg}^* according to the operating conditions. Ignoring the losses in the inverter, the active power on the AC side of the inverter is equal to the DC-side power, that is,

$$P_g = \frac{3}{2}v_{dg}i_{dg} = v_{dc}i_{dc} \qquad (4.29)$$

As previously mentioned, the power flow of the inverter system is bidirectional. When the active power is delivered from the grid to the DC circuit, the inverter operates in a rectifying mode $(P_g > 0)$, whereas when the power is transferred from the DC circuit to the grid $(P_g < 0)$, the inverter is in an inverting mode. The control system will automatically shift between the two operating modes and, therefore, no

extra measures should be taken for the controller. The DC load of the inverter can be modeled by a resistor R in series with a battery E to study the bidirectional power flow as shown in Figure 4-7. Since the average DC voltage V_{dc} of the inverter is set by its reference v_{dc}^{*} moreover, is kept constant by the PI controller, the direction of the power flow is set by the difference between E and V_{dc} according to the following conditions

$$\begin{cases} E < V_{dc} \Rightarrow I_{dc} > 0 \Rightarrow P_g > 0 \Rightarrow \text{Power from the grid to load (rectifying mode)} \\ E > V_{dc} \Rightarrow I_{dc} < 0 \Rightarrow P_g < 0 \Rightarrow \text{Power from load to grid (inverting mode)} \\ E = V_{dc} \Rightarrow I_{dc} = 0 \Rightarrow P_g = 0 \Rightarrow \text{No power flow between DC circuit and grid} \end{cases} \quad (4.30)$$

To determine an appropriate DC voltage reference v_{dc}^{*}, one should take system transients and possible grid voltage variations into account.

$$V_{dc}^{*} = \frac{\sqrt{6}V_{ai1}}{m_a} \quad (4.31)$$

4.2.2 VOC with Decoupled Controller

To further investigate the VOC scheme, the state equation for the grid-side circuit of the inverter in the abc stationary reference frame can be expressed as

$$\begin{cases} \frac{di_{ag}}{dt} = (v_{ag} - v_{ai})/L_g \\ \frac{di_{bg}}{dt} = (v_{bg} - v_{bi})/L_g \\ \frac{di_{cg}}{dt} = (v_{cg} - v_{ci})/L_g \end{cases} \quad (4.32)$$

Equation (4.32) can be transformed into the dq synchronous reference frame

$$\begin{cases} \frac{di_{dg}}{dt} = (v_{dg} - v_{di} + \omega_g L_g i_{qg})/L_g \\ \frac{di_{qg}}{dt} = (v_{qg} - v_{qi} - \omega_g L_g i_{dg})/L_g \end{cases} \quad (4.33)$$

where ω_g is the speed of the synchronous reference frame, which is also the angular frequency of the grid, and $\omega_g L_g i_{qg}$ and $\omega_g L_g i_{dg}$ are the induced speed voltages due to the transformation of the three-phase inductance L_g from the stationary reference frame to the synchronous frame.

Equation (4.33) illustrates that the derivative of the d-axis line current i_{dg} is related to both d-and *q*-axis variables, as is the q-axis current i_{qg}. This shows that the system control is cross-coupled, which may lead to problems in controller design and unsatisfactory dynamic performance. To resolve the problem, a decoupled controller shown in Figure 4-8 can be implemented.

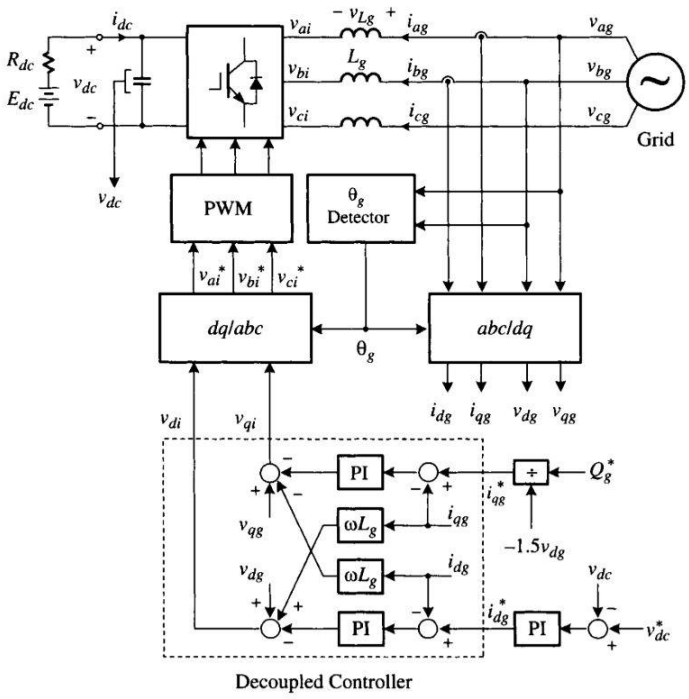

Figure 4-8 Voltage-oriented control (VOC) with a decoupled controller [9]

It is assumed that the controllers for the dq-axis currents in Figure 4-8 are of the PI type, the output of the decoupled controller can be expressed as

$$\begin{cases} v_{di} = -\left(k_1 + \dfrac{k_2}{s}\right)\left(i_{dg}^* - i_{dg}\right) + \omega_g L_g i_{qg} + v_{dg} \\ v_{qi} = -\left(k_1 + \dfrac{k_2}{s}\right)\left(i_{qg}^* - i_{qg}\right) - \omega_g L_g i_{dg} + v_{qg} \end{cases} \tag{4.34}$$

where $\left(k_1 + \frac{k_2}{s}\right)$ is the transfer function of the PI controller.

Substituting (4.34) into (4.33) yields

$$\begin{cases} \dfrac{di_{dg}}{dt} = \left(k_1 + \dfrac{k_2}{s}\right)\left(i_{dg}^* - i_{dg}\right)/L_g \\ \dfrac{di_{qg}}{dt} = \left(k_1 + \dfrac{k_2}{s}\right)\left(i_{qg}^* - i_{qg}\right)/L_g \end{cases} \tag{4.35}$$

Equation (4.35) indicates that the control of the d-axis grid current i_{dg} is decoupled, involving only d-axis components, as is the q-axis current i_{qg}. The decoupled control forms the design of the PI controllers more convenient, and the system is more easily stabilized.

5 Analysis of Case Studies

5.1 A Single Machine Equivalent

The simulated behavior of a wind turbine operating at the rated operational point will be representative of the collective response of the large wind farm at rated operation. The reason behind this is that the wind turbines in the large wind farm show a coherent response when subjected to a transient event in the power system [11].

According to [34], A large wind farm can merely be represented by a single machine equivalent in the analysis of voltage stability. A single machine equivalent means that a single wind turbine model represents a large wind farm. The following assumptions apply here:

- The capacity of the single machine equivalent is the sum of the power capacities of the wind turbines in the wind farm [35].
- The power supplied by the single machine equivalent is the sum of the power of the wind turbines in the wind farm [35].
- According to Danish specifications, the reactive power of the single machine equivalent is zero at the connection point [36].
- The risk of mutual interaction between the converter control system of Type D wind turbine is eliminated by efficient tuning of them [37].

Using single machine equivalent rather than a detailed model of a wind farm with many wind turbines can reduce the complexity of the voltage stability analysis. This simplification is also reasonable because conventional power plant units are commonly represented in the analysis of voltage stability by their lumped, single machine equivalents [34], [38].

In this thesis, DIgSILENT© PowerFactory composite model of the FullyRatedConv WTG 5.0 MW 50Hz is modified to generate 100 MW active power, which is then fed to the regional grid of Northern Norway. Parameters for different components present in this model are taken from DIgSILENT© PowerFactory model of 15 MW wind farm containing 6 Wind turbines with fully-rated converters. Also, test system developed by SINTEF, which was used in a technical report to analyze system requirements for wind power plants, was a source of some component's parameters [18]. Table A - 1 (given in Appendix A) contained parameter values of component used to build this model.

Also, Table A - 2 (given in Appendix A) shows power generated by WT concerning wind speed. Inbuilt DIgSILENT© PowerFactory Wind Power Curve has inspired mentioned table.

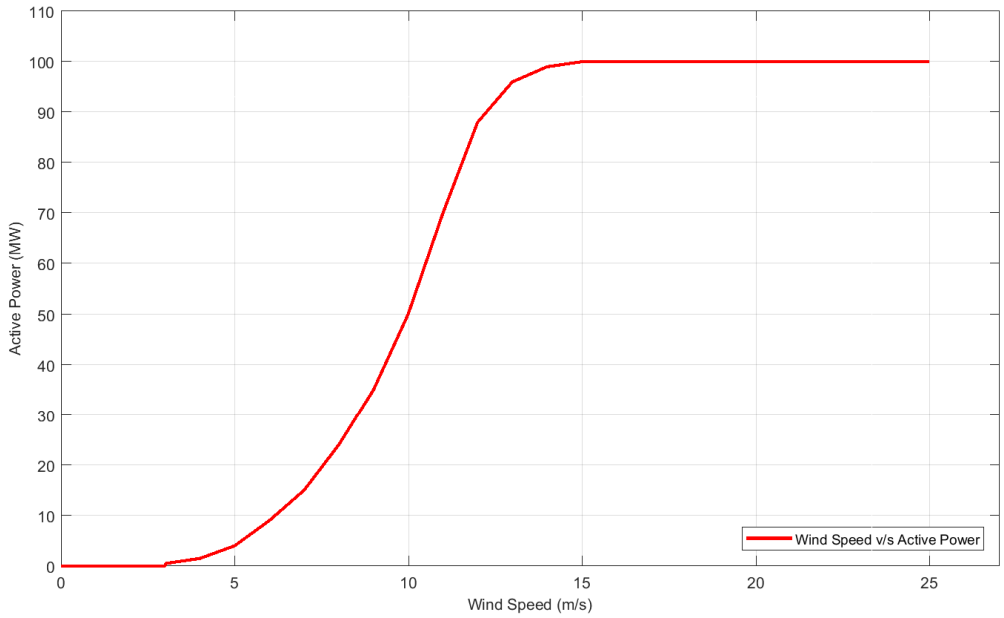

Figure 5-1 Power curve of Wind Turbine

Figure 5-1 shows power curve which describes the overall performance of the wind turbine. The power curve relates the steady-state output power developed by the wind turbine to the free wind speed. It is generally measured using 10-minutes average data. The wind turbine remains shut down below the cut-in speed of about 3 m/s because the power in the wind is very low for useful energy production. Then, once operating, the output power increases following a broadly cubic relationship with wind speed until rated wind speed is reached. Above rated wind speed, the aerodynamic rotor is arranged to limit the mechanical power extracted from the wind and so reduce the mechanical loads on the drive train. The wind turbine is shut down in very high wind speeds.

The choice of cut-in, rated and shutdown wind speeds are made by the wind turbine designer who will try to balance maximum energy extraction with controlling the mechanical loads of the turbine.

5.2 General Information regarding Model

In DIgSILENT © PowerFactory software, Single-line schematic Diagram representation of systems is used. The connecting lines between two consecutive busbars signify three-phase system. It is much easier to work with Single-line schematic Diagram than three phase models. The model is comprised of Full Converter Wind Turbine which integrated to the Grid through different power system's component as presented in case studies below. The model shows a lumped turbine injecting 100 MW active power to 1 kV LV connection. Then a transformer of rating 112 MVA is used to step up the voltage to 22 kV. The underground cable of 0.5 km transfers the power to the wind farm's boundary, where the voltage again steps up to 132 kV through 150 MVA rating transformer. After that, power is fed into the external grid by using 50 km 132 kV overhead transmission line. The external grid is modeled as a slack bus.

Information displays on connecting line represent active power, reactive power, and line current. Moreover, Information appears on busbar represents line to line voltage, its pu value, and voltage angle. It applies to all case studies performed below. The wind turbine generator is connected to Low-Voltage (LV) connection having 1 kV line-to-line voltage. External Grid is tied with Bus 1 which is having 132 kV line-to-line voltage. Negative sign shows the flow of active or reactive power into the External Grid, whereas positive sign indicates the opposite scenario. Change in color of busbars represents its voltage fluctuation concerning its defined base value. Dark green color represents busbar voltage 1 pu, and different color appears according to DIgSILENT © PowerFactory software inbuilt heatmap settings. This feature also applies to the power system components where black shows the loading of the component is the underdefined limit. However, red color indicates the component is loaded heavily and working near to its full capacity power rating. Small boxes on connecting lines represent the circuit breaker so that circuit can be opened by merely by double-clicking on them. Moreover, Small circles on busbars imply connecting nodes.

Case Study 1

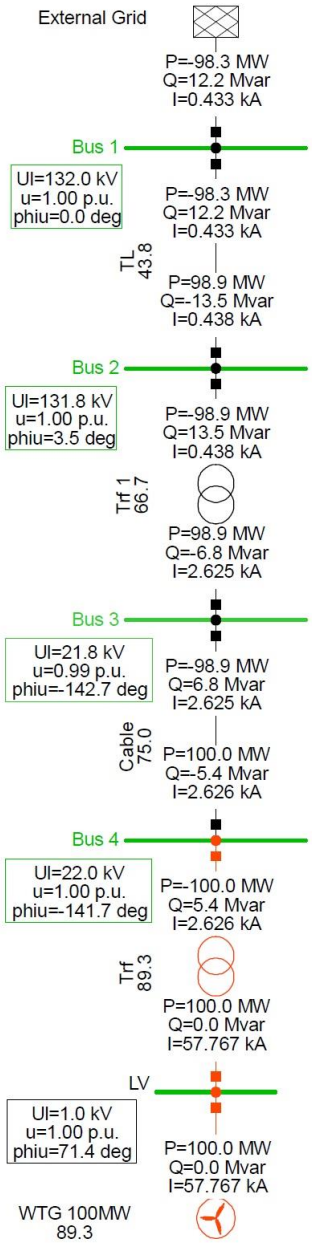

Figure 5-2 WES model without reactive power generation

It can be seen in Figure 5-2 that wind turbine is generating 100 MW of active power and no reactive power at 1 kV output voltage. Considering higher values of voltage at the output terminal of WT reduces the line current, and hence the losses reduction. On the other side at Bus 1, 98.3 MW of active power is received by the grid after considering active power losses of the system. Since, in this case, the wind turbine is not participating in reactive power generation, 12.2 MVAr reactive power is taken from the External Grid to magnetize the system's components primarily transformers. It is also observed that 50 km regional transmission line generates around 1.3 MVAr reactive power due to Ferranti effect.

Case Study 2

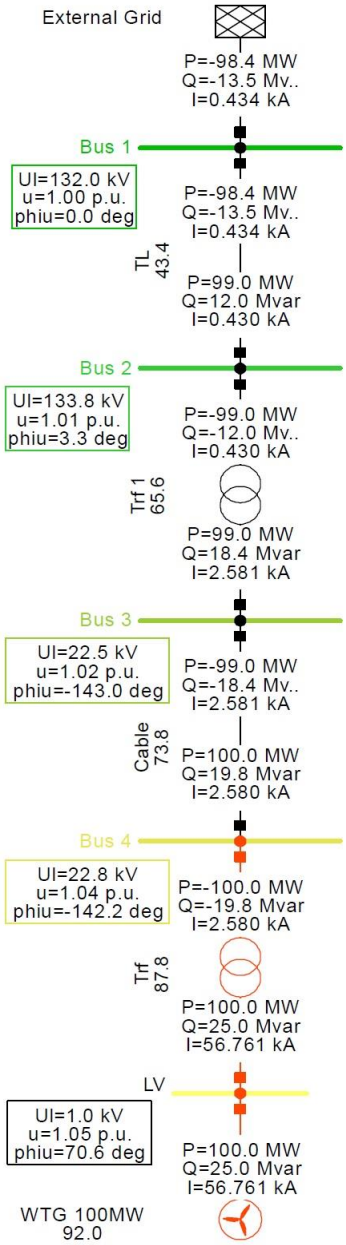

Figure 5-3 WES model with 25 MVAr reactive power generation

Figure 5-3 shows the modified model of the WT to generate reactive power by controlling grid-side 2L-VSC. Grid-side inverter control is modified in a way that it should fulfill the reactive power requirement of the system and, in addition to that, it should provide reactive power to the grid as well. The WT generates 25 MVAr of reactive power, and 11.5 MVAr is used for system purpose, and rest is transferred to the grid (13.5 MVAr). It is calculated that around 700 kVAr reactive power consumption of the system is reduced due to local reactive power generation. 98.4 MW of active power reached to the External Grid after considering active power losses.

Case Study 3

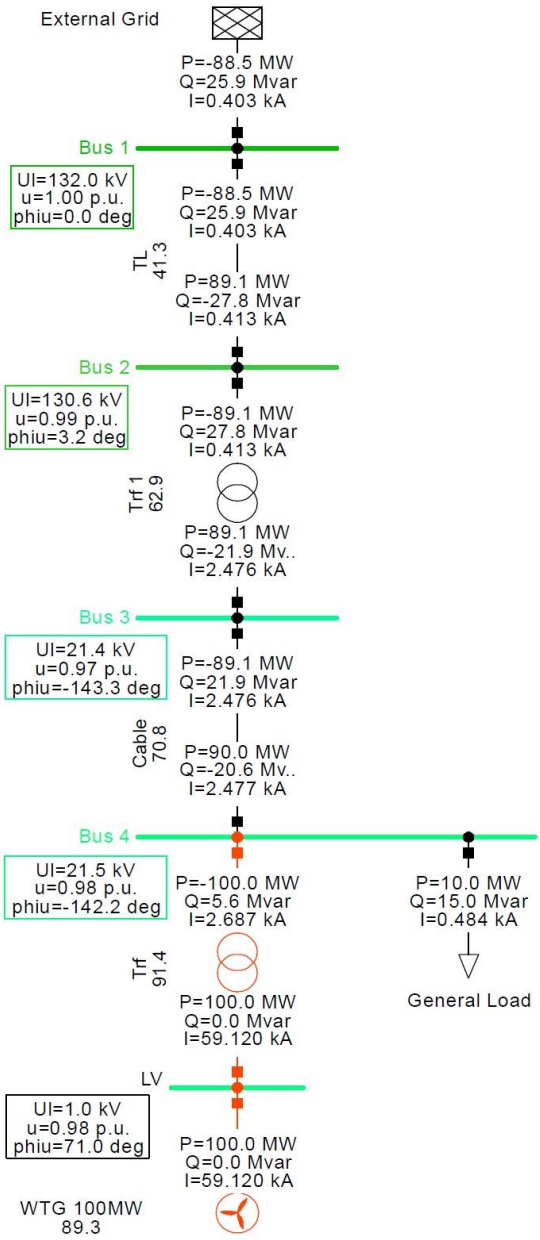

Figure 5-4 WES model considering general load at Bus 4, No reactive power generation

As shown in Figure 5-4, a general load is placed at Bus 4. The load is consuming 10 MW active power and 15 MVAr reactive power. This case study is done to check the feasibility of the system. Wind Turbine transfers 88.5 MW active power to the grid after fulfilling the load requirement and system losses. However, WT must borrow reactive power from the grid in order to provide to the general load and its own system's components. The voltage drop on all busbars below Bus 3 is the vital observation to mention here. This occurs due to lack of reactive power supply. Since voltage and reactive power are directly related to one another, voltage drops to 21.4 kV and 21.5 kV at Bus 3 and Bus 4, respectively. Hence, two ways, out of many, are considered to compensate this reactive effect.

Case Study 4

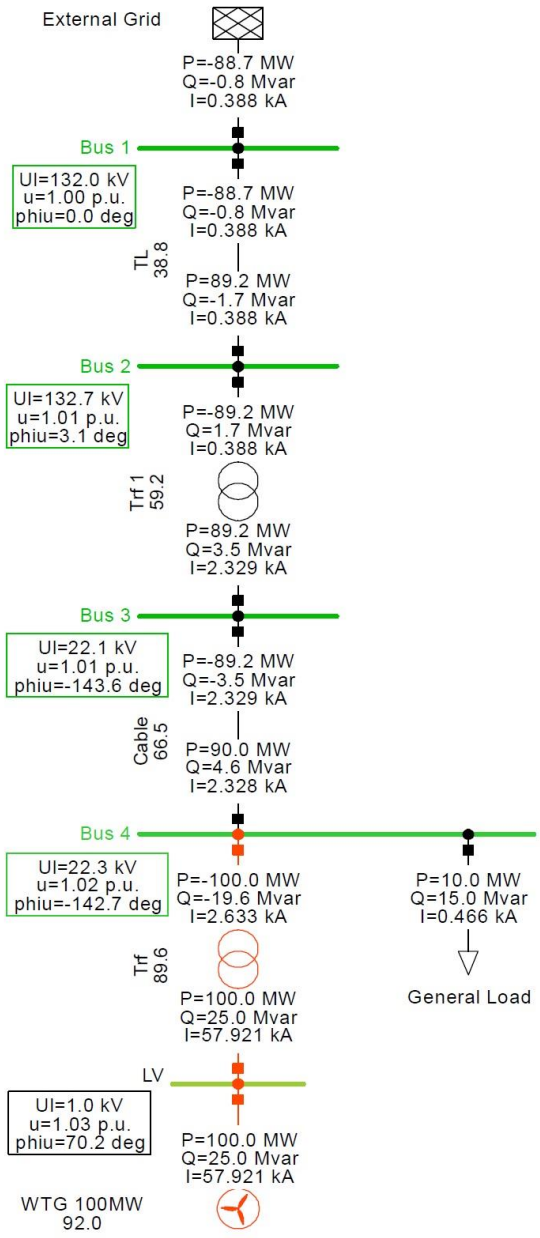

Figure 5-5 WES model considering general load at Bus 4, 25 MVAr reactive power generation

To raise the voltage at busbars as mentioned above, Wind Turbine should produce reactive power. Figure 5-5 illustrates the system in which WT provides 25 MVAr reactive. Therefore, the voltage has been raised above. Furthermore, 800 kVAr reactive power is supplied to the external grid as shown above after accomplishing reactive power requirement of the system. It is also noted that there is raise of 200 kW active power which is transferred to the grid. So, it became 88.7 MW instead of 88.5 MW which was in case study 3.

Case Study 5

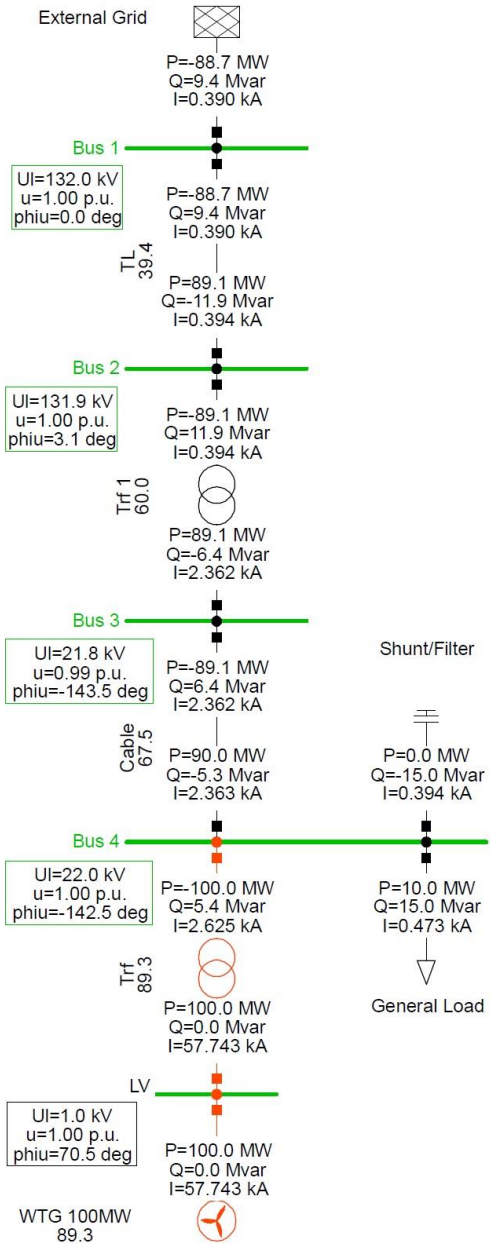

Figure 5-6 WES model considering general load and VAR generator of 15 MVAr at Bus 4

In this case study, a VAR generator is placed at Bus 4. It provides the same amount of reactive power which load requires (15 MVAr) as shown in Figure 5-6. It is observed that Bus 4 voltage became 1 pu by doing this. Hence, voltage stability is achieved is sometimes called load stability also. Moreover, system requirement of reactive power is much lesser as compared to case study 1. It is 9.4MVAr in the current case. However, it was 12.2 MVAr in case study 1. It is noticed that it is better option to provide shunt compensation locally than receiving from generating end through long transmission line networks. The reason is defined by mentioning one of many drawbacks of low power factor in the system.

The main disadvantage of low power factor:

- High MVA rating of system's component

Considering general load chosen in above case studies, it is calculated that load is having a power factor of approx. 0.55. The power factor of the load is lagging because of dominating reactive power consumption of the load. As it is known that the apparent power can be defined as

$$\text{Apparent Power} = \frac{\text{Active Power}}{\text{Power Factor}} \tag{5.1}$$

Power factor is inversely proportional to the apparent power as shown in Equation (5.1). Hence, the apparent power rating of components in the system increases due to low power factor. However, power factor can be significantly improved by placing a VAR generator which is having a capacitance of 91.74μF and inductance of 7.73mH at Bus 4. It also helps to reduce system cost since high MVA rating transformers, circuit breaker, isolator, and so on are very expensive. It is best to have unity power factor, so maximum active power can be transferred from sending to receiving end. Therefore, Reactive power compensation of wind turbines is usually provided by shunt capacitor banks, SVC or AC/DC/AC converters.

6 Discussion and Conclusion

Firstly, a different type of wind turbine technologies has been analyzed and compared according to their advantages and disadvantages. At the beginning of this thesis work, Type D (Variable-speed WT with Full-Capacity Power Converter) wind turbine technology has been decided to work on. Therefore, Full converter technology combined with squirrel cage induction generator has been preferred over its associate competitor design technologies. Also, this technology is dominating the contemporary market.

Different approaches have been performed to attain the required objectives of this thesis. In the beginning, Simulink has been used. However, later, DIgSILENT © PowerFactory has been preferred over Simulink due to its full range of functionality from standard features to highly sophisticated and advanced applications.

Secondly, this thesis covered symmetrical steady-state analysis of the wind farm when connecting to the grid. Load flow studies have been performed considering Active power generation, $P_g = 100\text{MW}$ and Reactive power generation, $Q_g = 0 \text{ and } 25$ MVAr. Moreover, a general load consuming active power and reactive power of 10 MW and 15 MVAr, respectively has been included in last three case studies to analyze the feasibility of the system more deeply. In case study 3 and 4, wind turbine generator generates reactive power, $Q_g = 0 \text{ and } 25$ MVAr, respectively. Nevertheless, in case study 5, VAR generator (Shunt compensation having a capacitance of 91.74µF and inductance of 7.73mH) is connected to load bus to stabilize the voltage by providing 15 MVAr reactive power to the load. Case studies results are discussed above. Graphs which drawn at generation and grid busbars are included in Appendix B.

It is known that load flow study is the steady-state solution of the power system network. The critical information obtained from this study comprises the magnitude and phase angle of the bus voltages, reactive power at generator buses, real and reactive power flow on transmission lines, other variables being specified. This information is vital for continuous monitoring of the current state of the system and for analyzing the effectiveness of alternative plans for future system expansion to meet increased load demand.

Thirdly, efforts had been made to achieve transient stability analysis as well. In the beginning, it was believed that performing these studies will be much more straightforward in DIgSILENT © PowerFactory as compared to Simulink. However, unfortunately, the approach was unsuccessful because of very high complexity in the DIgSILENT © PowerFactory. Though it turned out to be other way around. In addition to this, it took some time to get to know about the software. Since full access had been achieved quite late, lack of time was another factor affected at the end.

It is essential to achieve transient stability analysis because power systems are vast nowadays. They are densely interconnected with thousands of machines which interacts through the medium of extra-high-voltage (EHV) and ultra-high-voltage (UHV) networks. These machines have associated excitation systems and turbine-governing control systems which in some cases are modeled to reflect the appropriately correct dynamic performance of the system. Moreover, transient stability analysis of a system is significant when considering different types of faults which occur in the grid. Effect of these faults should be observed on system's components especially machines behavior in these cases. Therefore, a different type of faults should be created to perform short circuit analysis. These faults can be classified as small and large disturbances. A change in the gain of the automatic voltage regulator in the excitation system of a large generating unit could be an example of a small disturbance. However, sudden changes in load, transmission system faults, loss of generating units, and line switching are examples of large disturbances.

6.1 Future work

- Transient stability analysis can be the next task for this research work. Especially, transient voltage stability of wind energy system can be considered. Since the output power of the wind turbine generator generally varies significantly within a time of a few seconds due to incoming wind speed variations, viable measures can be exploited to enable secure operation of the system close to the thermal capacity and stability limits.
- Furthermore, market integration can be analyzed. Since many interconnectors are being built to have European super grid, Norwegian wind power can be sold in European electricity markets with higher prices when there is a shortage of power supply in these areas.

References

[1] P. A. C. Rosas, *Dynamic Influences of Wind Power on The Power System*. 2004.

[2] T. Aigner, S. Jaehnert, G. L. Doorman, and T. Gjengedal, "The Effect of Large-Scale Wind Power on System Balancing in Northern Europe," *IEEE Trans. Sustain. Energy*, vol. 3, no. 4, pp. 751–759, 2012.

[3] Statkraft, "Europe's largest onshore wind power project to be built in Central-Norway." [Online]. Available: https://www.statkraft.com/IR/stock-exchange-notice/2016/europes-largest-onshore-wind-power-project--to-be-built-in-central-norway--/. [Accessed: 05-Jun-2018].

[4] NVE, "Vannkraft." [Online]. Available: https://www.nve.no/energiforsyning-og-konsesjon/vannkraft/. [Accessed: 04-Jun-2018].

[5] NVE, "Vannkraftpotensialet." [Online]. Available: https://www.nve.no/energiforsyning-og-konsesjon/vannkraft/vannkraftpotensialet/. [Accessed: 04-Jun-2018].

[6] T. Gjengedal, "Large-scale wind power farms as power plants," *Wind Energy*, vol. 8, no. 3, pp. 361–373, Jul. 2005.

[7] D. E. ; A. N. Weir, "Vindkraft - produksjon i 2017."

[8] E. Hau, *Wind turbines: Fundamentals, technologies, application, economics*, vol. 9783642271. 2013.

[9] B. Wu, Y. Lang, N. Zargari, and S. Kouro, *Power Conversion and Control Of Wind Energy Systems*. 2011.

[10] F. Blaabjerg and Z. Chen, "Power Electronics for Modern Wind Turbines," *Synth. Lect. Power Electron.*, vol. 1, no. 1, pp. 1–68, 2006.

[11] T. Ackermann, *Wind Power in Power Systems*, vol. 140, no. February. 2005.

[12] I. Boldea, *Variable Speed Generators*. 2006.

[13] R. C. Bansal, "Three-phase self-excited induction generators: An overview," *IEEE Transactions on Energy Conversion*, vol. 20, no. 2. pp. 292–299, 2005.

[14] D. J. Burnham, S. Santoso, and E. Muljadi, "Variable rotor-resistance control of wind turbine

generators," *2009 IEEE Power Energy Soc. Gen. Meet.*, 2009.

[15] B. Fox, Ebooks Corporation., and Ebook Library., *Wind Power Integration : Connection and System Operational Aspects*. 2007.

[16] E. Hagstrøm, I. Norheim, and K. Uhlen, "Large-scale wind power integration in Norway and impact on damping in the Nordic grid," *Wind Energy*, vol. 8, no. 3, pp. 375–384, 2005.

[17] M. Tsili and S. Papathanassiou, "A review of grid code technical requirements for wind farms," *IET Renew. Power Gener.*, vol. 3, no. 3, pp. 308–332, 2009.

[18] K. Uhlen, "System Requirements for Wind Power Plants," Trondheim, Norway, 2007.

[19] N. R. Ullah, T. Thiringer, and D. Karlsson, "Voltage and transient stability support by wind farms complying with the E.ON netz grid code," *IEEE Trans. Power Syst.*, vol. 22, no. 4, pp. 1647–1656, 2007.

[20] M. Altin, Ö. Göksu, R. Teodorescu, P. Rodriguez, B. B. Jensen, and L. Helle, "Overview of recent grid codes for wind power integration," in *Proceedings of the International Conference on Optimisation of Electrical and Electronic Equipment, OPTIM*, 2010, pp. 1152–1160.

[21] V. Le, X. Li, Y. Li, T. L. T. Dong, and C. Le, "An innovative control strategy to improve the fault ride-through capability of DFIGs based on wind energy conversion systems," *Energies*, vol. 9, no. 2, pp. 1–23, 2016.

[22] P. Gardner, S. Mcgoldrick, T. Higgins, and B. Ó. Gallachóir, "The effect of increasing wind penetration on the electricity systems of the Republic of Ireland and Northern Ireland," in *Proceedings of the European Wind Energy Conference 2003*, 2003, p. 7.

[23] S. Heier, *Grid Integration of Wind Energy*. 2014.

[24] B. Wu and M. Narimani, *High-Power Converters and AC Drives: Second Edition*. 2016.

[25] P. C. Krause, O. Wasynczuk, and S. D. Sudhoff, "Analysis of Electric Machinery and Drive Systems," *Power Eng.*, pp. 1–65, 2002.

[26] N. Mohan, "Dynamic Analysis of Induction Machines in Terms of dq Windings," in *Advanced Electric Drives*, 2014, pp. 28–58.

[27] B. K. Bose, "Power Electronics And Motor Drives," *Power Electron. Mot. Drives*, vol. 56, no. 2, pp. 649–729, 2006.

[28] H. Geng, D. Xu, B. Wu, and W. Huang, “Direct voltage control for a stand-alone wind-driven self-excited induction generator with improved power quality,” *IEEE Trans. Power Electron.*, vol. 26, no. 8, pp. 2358–2368, 2011.

[29] O. Anaya-Lara, N. Jenkins, J. Ekanayake, P. Cartwright, and M. Hughes, *Wind energy generation : modelling and control*, vol. 54, no. 2. 2009.

[30] N. Mohan, T. M. Undeland, and W. P. Robbins, *Power Electronics Converters, Applications, and Design*, vol. 4. 2007.

[31] M. A. Boost and P. D. Ziogas, “State-of-the-Art Carrier PWM Techniques: A Critical Evaluation,” *IEEE Trans. Ind. Appl.*, vol. 24, no. 2, pp. 271–280, 1988.

[32] J. Holtz, “Power electronics-A continuing challenge,” *IEEE Ind. Electron. Mag.*, vol. 5, no. 2, pp. 6–15, 2011.

[33] M. H. Rashid, *Power Electronics Handbook*. 2007.

[34] T. Gjengedal, “Modeling and Aggregation of Wind Parks for Power System Stability Studies,” in *Proc. of the 5th WSEAS/IASME Int. Conf. on Electrical Power Systems, High Voltages, Electrical Machines*, 2005, pp. 480–485.

[35] V. Akhmatov and H. Knudsen, “An aggregate model of a grid-connected, large-scale, offshore wind farm for power stability investigations - Importance of windmill mechanical system,” *Int. J. Electr. Power Energy Syst.*, vol. 24, no. 9, pp. 709–717, 2002.

[36] Eltra and Elkraft, “Wind turbines connected to grids with voltages below 100 kV,” *Http://Www.Eltra.Dk*, no. May, 2004.

[37] J. G. Slootweg and W. L. Kling, “Impacts of distributed generation on power system transient stability,” *Power Engineering Society Summer Meeting, 2002 IEEE*, vol. 2. pp. 862–867 vol.2, 2002.

[38] V. Akhmatov, *Analysis of dynamic behaviour of electric power systems with large amount of wind power*, vol. Ph.D in El, no. April. 2003.

Appendix A

Table A - 1 Main components of the model [18]

Components	**Node(s)**	**Capacity / rating**	**Comments**
Wind Farm	Bus 4	100 MW	Single Machine Equivalent. 2L-VSC SCIG Configuration.
Radial Cable connecting the Wind Farm	Bus 3 – Bus 4	22 kV R = 0.102 Ω/km X = 0.168 Ω/km C_d = 3.68 µF/km	0.5 km
Transmission Line	Bus 1 – Bus 2	132 kV R = 0.021 Ω/km X = 0.210 Ω/km C_d = 26.52 ηF/km	50 km

Table A - 2 Active Power corresponding to Wind Speed

Wind Speed (m/s)	**Active Power (MW)**
0	0
1	0
2	0
3	0
3.01	0.5
4	1.5
5	4
6	9
7	15
8	24
9	35
10	50
11	70
12	88
13	96
14	99
15	100
16	100
17	100
18	100
19	100
20	100
21	100
22	100
23	100
24	100
25	100

Appendix B

Case Study 1

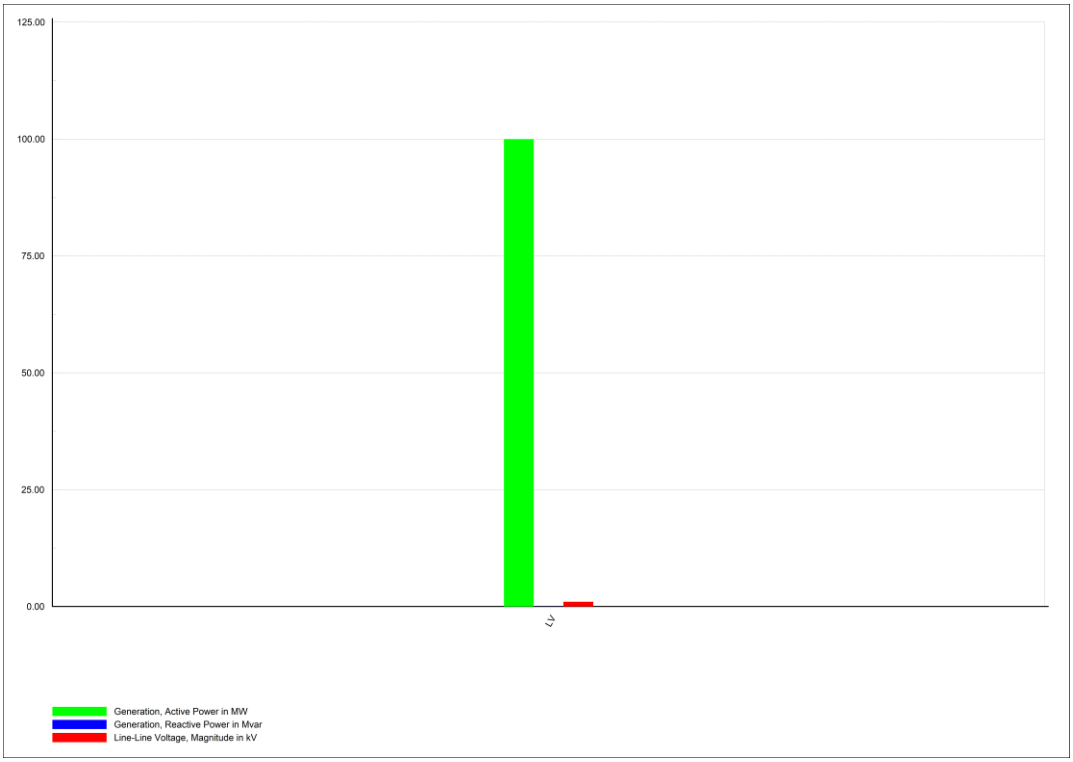

Figure B - 1 WT Power Generation at LV

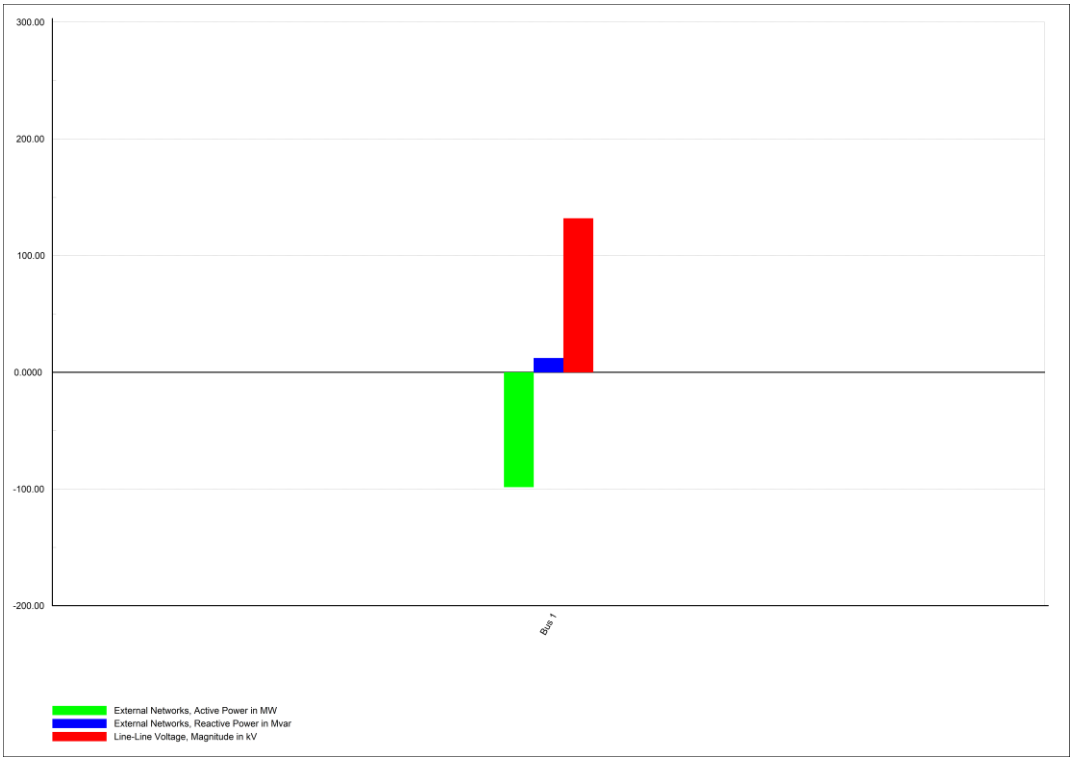

Figure B - 2 Power transfer at Bus 1

Case study 2

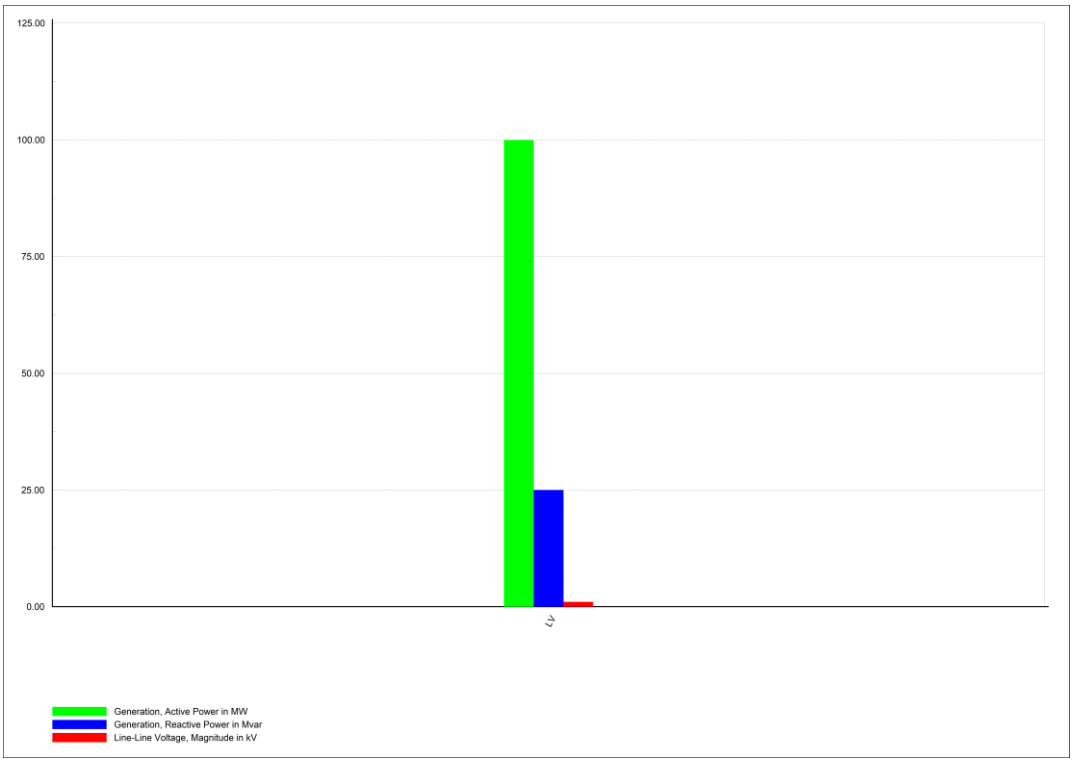

Figure B - 3 WT Power Generation at LV

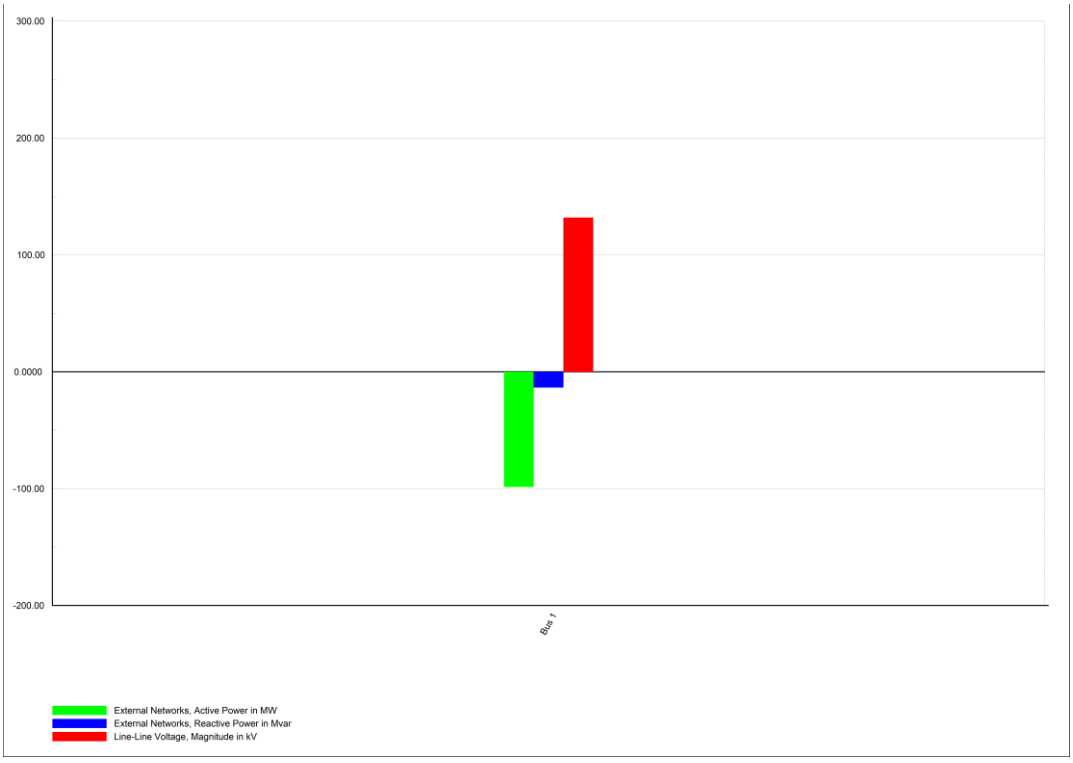

Figure B - 4 Power transfer at Bus 1

Case study 3

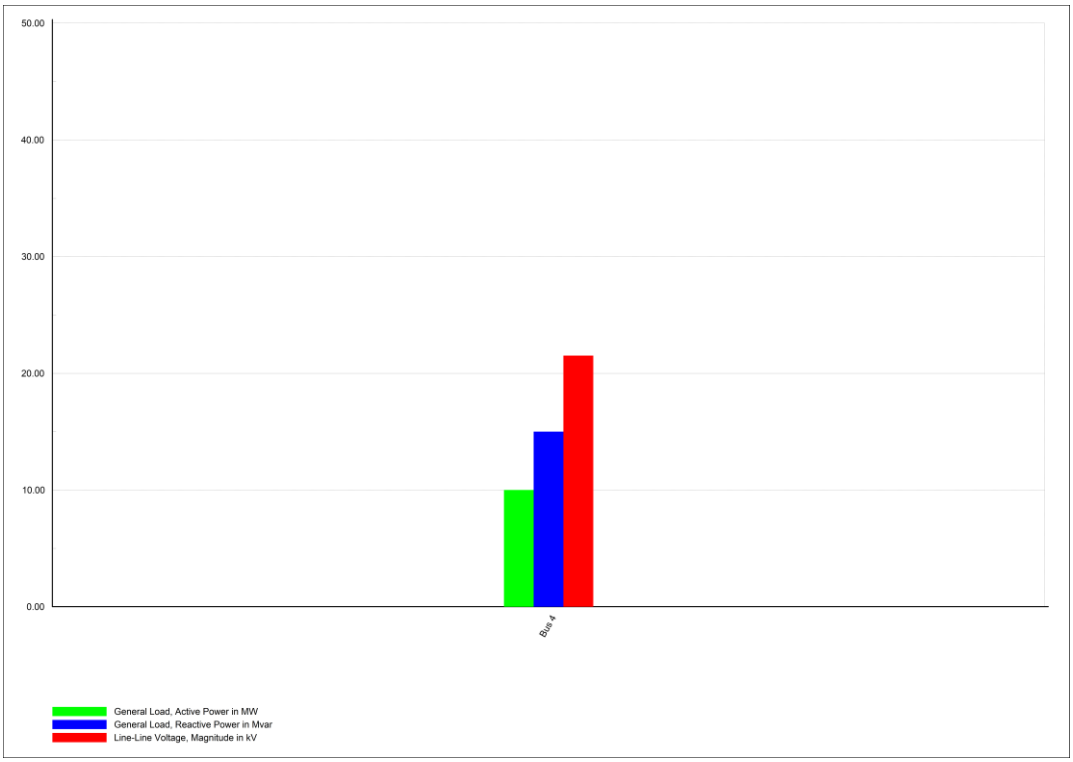

Figure B - 5 Power demand of General Load at Bus 4

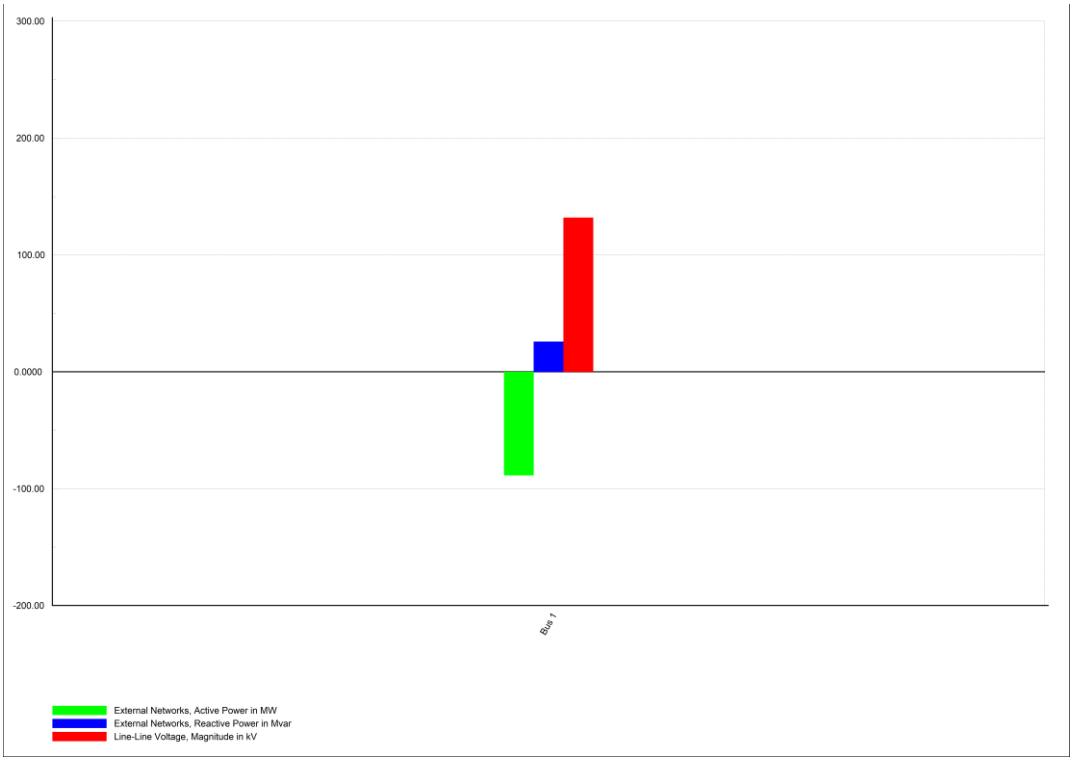

Figure B - 6 Power transfer at Bus 1 after fulfilling load demand

Case study 4

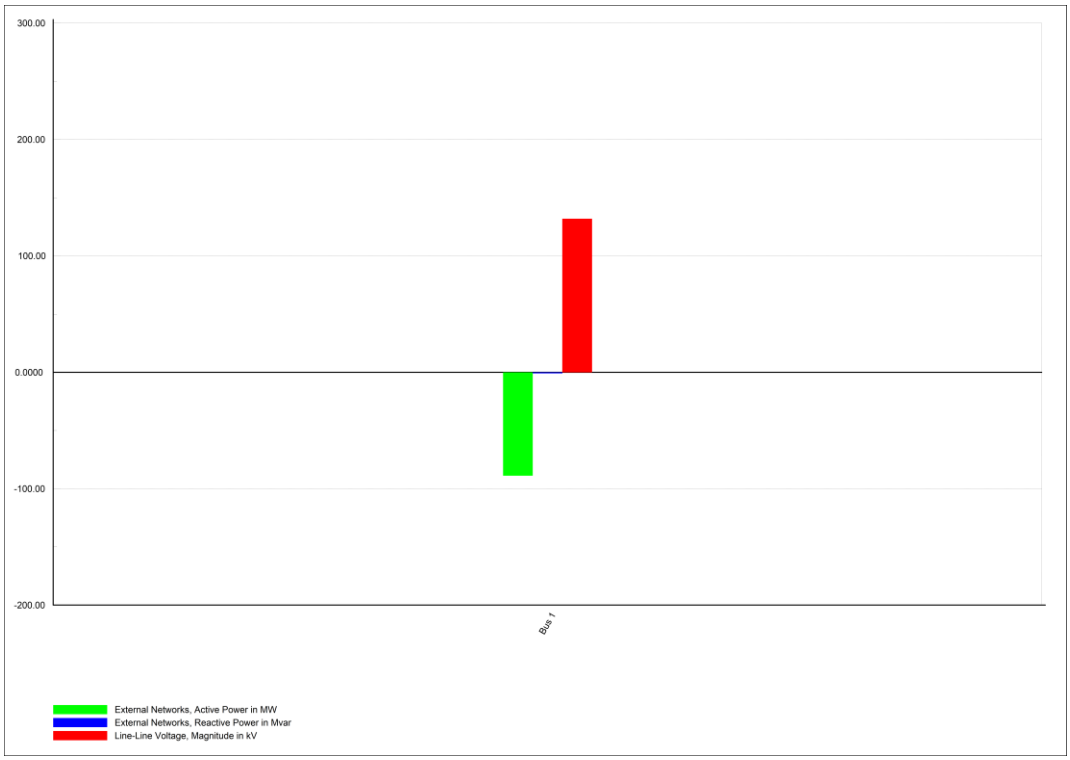

Figure B - 7 Power transfer at Bus 1 after considering load power requirement

Case study 5

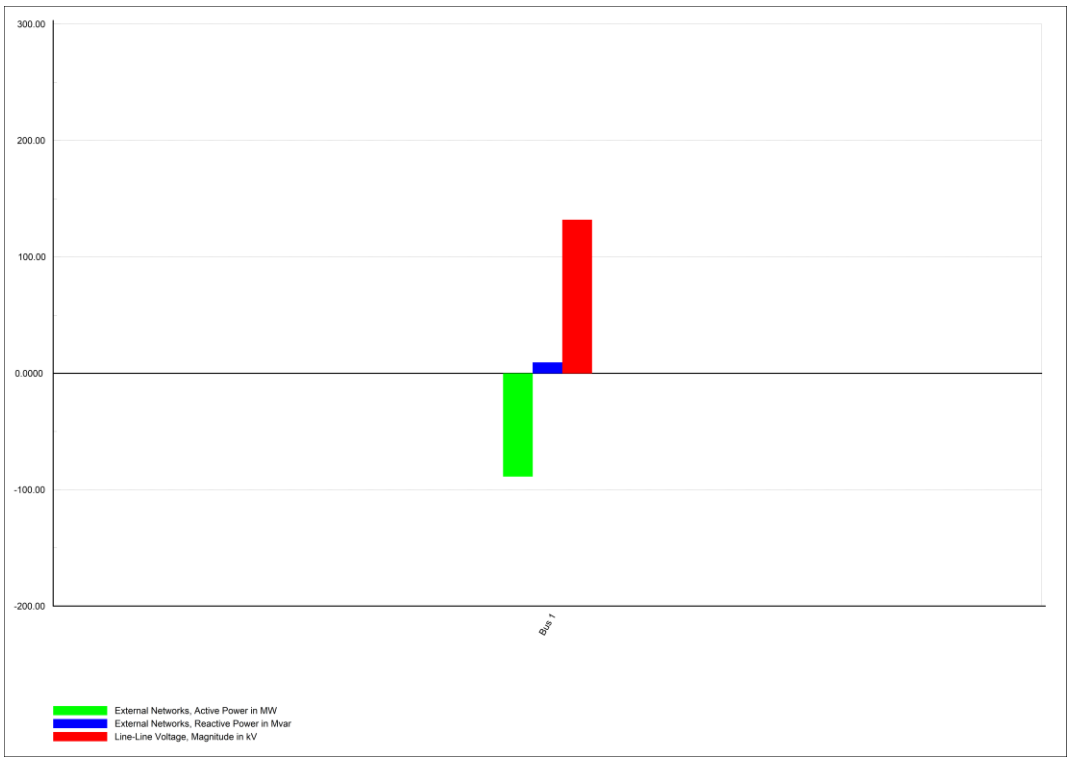

Figure B - 8 Power transfer at Bus 1 after installing VAR generator at Bus 4